May 2003 • NREL/SR-520-33836

Subcontractor Report

Advanced CIGS Photovoltaic Technology

Annual Technical Report
15 November 2001–14 November 2002

A.E. Delahoy and L. Chen
Energy Photovoltaics, Inc.
Princeton, New Jersey

National Renewable Energy Laboratory

1617 Cole Boulevard
Golden, Colorado 80401-3393

NREL is a U.S. Department of Energy Laboratory
Operated by Midwest Research Institute • Battelle • Bechtel

Contract No. DE-AC36-99-GO10337

May 2003 • NREL/SR-520-33836

Advanced CIGS Photovoltaic Technology

Annual Technical Report
15 November 2001–14 November 2002

A.E. Delahoy and L. Chen
Energy Photovoltaics, Inc.
Princeton, New Jersey

NREL Technical Monitor: H.S. Ullal

Prepared under Subcontract No. ZDJ-2-30630-21

National Renewable Energy Laboratory

1617 Cole Boulevard
Golden, Colorado 80401-3393

NREL is a U.S. Department of Energy Laboratory
Operated by Midwest Research Institute • Battelle • Bechtel

Contract No. DE-AC36-99-GO10337

NOTICE

Available electronically at http://www.osti.gov/bridge

Available for a processing fee to U.S. Department of Energy
and its contractors, in paper, from:

U.S. Department of Energy
Office of Scientific and Technical Information
P.O. Box 62
Oak Ridge, TN 37831-0062
phone: 865.576.8401
fax: 865.576.5728
email: reports@adonis.osti.gov

Available for sale to the public, in paper, from:

U.S. Department of Commerce
National Technical Information Service
5285 Port Royal Road
Springfield, VA 22161
phone: 800.553.6847
fax: 703.605.6900
email: orders@ntis.fedworld.gov
online ordering: http://www.ntis.gov/ordering.htm

Printed on paper containing at least 50% wastepaper, including 20% postconsumer waste

Preface

Energy Photovoltaics, Inc. (EPV) has been engaged in the research and development of thin-film $Cu(In,Ga)Se_2$ (CIGS) photovoltaic technology since 1991. EPV has consistently pursued a vacuum-based approach to CIGS production, using novel linear source technology and standard soda-lime glass substrates. It has also chosen to develop processing methods with worker safety in mind. These choices result in layers having controllable purity and low physical defects, and production without significant hazards. Considerations such as these are important in helping to minimize the processing costs of CIGS.

Technically, thin film PV technologies have advanced considerably in the last few years [R1]. However, for technologies to survive, they must also perform well commercially [R2]. As a result of such fiscal pressures, we have recently witnessed BP Solar shutting down two sophisticated thin film lines, CdTe in Fairfield, CA, and a-Si,Ge in Toano, VA. At the time of writing, the leading commercially-available thin film technologies have demonstrated the following record aperture area efficiencies and powers for large area modules:

CIGS	12.5%	74.0W	Wurth Solar
CIGSS	12.1%	44.3W	Shell Solar
CdTe	10.1%	67.1W	First Solar
a-Si/μc-Si (w. back reflector)	10.0%	38.0W	Kaneka
a-Si triple (w. back reflector)	7.9%	35.7W	United Solar
a-Si dual (w. back reflector)	6.1%	33.3W	RWE
a-Si dual (wo. back reflector)	5.7%	42.3W	Energy Photovoltaics

Even higher efficiencies have been demonstrated by some companies that currently do not use the technology commercially, e.g. 13.4% for a CIGS module by Showa Shell, and 11% for CdTe modules by BP Solar and Matsushita. It may be noted that CIGSS continues to hold the efficiency record.

If PV continues to grow at 30% per year for the next 30 years in order to take its place as a significant energy source on the world stage, then modules have to be made in a more energy-efficient manner. Under this growth scenario, for a new PV factory to generate a positive energy return in less than 10 years, the specific energy for module production must be less than $18MJ/W_p$ [R2]. The published range of total energy requirements to produce wafer-based modules is 20-100 MJ/W_p. For CIGS, the figure is $11MJ/W_p$ (Shell Solar), and for a-Si the figure is $12\text{-}15MJ/W_p$ (EPV). Considerations such as these must ultimately be reflected in the formulation of energy policies.

During its previous 3-year, cost-shared research subcontract with NREL that ended in November 2001, EPV successfully produced high quality 0.43m^2 Mo-coated glass substrates that, when cut up, enabled NREL to produce 17.1% CIGS cells on such substrates [1]. EPV further successfully utilized novel linear evaporative sources for supply of Cu, In, Ga and Se to form CIGS on 0.43m^2 substrates, producing modules with V_{oc}'s up to 37V. A new approach to buffer layer deposition was pioneered through synthesis of the compound $ZnIn_2Se_4$ and its use as a source material. In addition, the current generated in exploratory a-Si/a-Si/CIGS stacked devices was increased from 6 to 13 mA/cm^2. Supporting these programs, EPV's upgraded analytical laboratories provided rapid in-house feedback concerning material and device properties.

The current three-phase, cost-shared subcontract with NREL (ZDJ-2-30630-21) is entitled "Advanced CIGS Photovoltaic Technology." The subcontract is part of the NREL **Thin-Film Photovoltaics Partnership Program (TFPPP)**, and EPV participates in both the Absorber and Alternative Junctions segments of the National CIS Team Meetings. The objective of this subcontract is to develop and assemble the various pieces of new technology that EPV considers essential for cost-effective production of CIGS modules. The long-term objective of the TFPPP is to demonstrate low-cost, reproducible modules of 15% aperture area efficiency. This annual technical report describes the major results obtained during the first phase of the subcontract (November 15, 2001 - November 14, 2002).

CONTENTS

TABLES

FIGURES

1.0 Introduction

As part of the Thin Film Photovoltaics Partnership Program, Energy Photovoltaics, Inc. has conducted research to help generate and support a technology base for production of CIGS PV modules based on vacuum deposition onto glass. To prepare CIGS on large glass substrates (currently 0.43m^2, with a projected further scale up to 0.79m^2), EPV has developed novel technology to deliver materials from stationary line sources to moving substrates.

This strategy was chosen after observing that, despite there being several methods of forming device quality CIGS (e.g. vacuum deposition, atmospheric pressure selenization of metallic precursors, rapid thermal processing, and electrodeposition), vacuum deposition has repeatedly achieved the world record for the highest efficiency CIGS device. Thus, in 1998, a record thin-film solar cell efficiency (18.8% for 0.44 cm^2) was achieved by NREL using vacuum-deposited CIGS [R3]. The deposition employs four point sources and flux integration for process control. In November 2002, this record was broken again by NREL with the announcement of a 19.2% device. In an attempt to overcome barriers to manufacturing CIGS by vacuum deposition, EPV has developed vacuum equipment incorporating novel linear evaporation sources designed for uniform coating of large substrates [2]. The use of elemental selenium avoids the need for gaseous H_2Se and makes for a safe manufacturing environment.

Project Objective: There are many objectives of this R&D program. One is to develop CIGS and junction formation recipes capable of producing small area devices with efficiencies in the range 14-16%. In this activity, the CIGS component of the cell will be prepared only by methods capable of immediate implementation on EPV's large scale processing equipment. Objectives related to the large-scale equipment include improvement of the uniformity of thickness and composition of layers produced by the linear sources, deposition control, and fabrication of large area modules with efficiencies up to 10%. The method of junction formation is of particular interest, and desirably should replace the traditional CBD CdS step. Two further major operations in which advances are sought are high rate deposition of high quality doped ZnO, and patterning operations that exhibit low area and electrical losses. Other objectives relate to module reliability testing, and improved materials utilization. These goals were chosen to provide a foundation for manufacturing of CIGS modules using wholly or mostly vacuum processing for layer deposition.

Approach: R&D and process development for CIGS is conducted in the Hercules 4-source system (six 5cm x 10cm stationary substrates per run) and in the Zeus 4-source system (one 4300 cm^2 moving substrate per run). In the latter system, which is load locked, source materials are delivered downwards to the moving glass using custom-built source heads housing four independent linear evaporative sources, the source axes being perpendicular to the direction of glass travel. This approach allows a wide range of vacuum-based CIGS recipes to be implemented. Copper can be supplied either by thermal evaporation or by planar-magnetron sputtering in a separate in-line deposition system. The integration of Cu sputtering into the Zeus system is planned.

For junction formation, EPV relies on CBD CdS on a day-to-day basis, while exploring alternative methods in parallel. Other methods include buffer layers applied by evaporation of $ZnIn_2Se_4$ (or other materials) and buffer layers applied by spray deposition. For ZnO deposition,

two planar-magnetron sputtering systems are available and are fitted with ceramic ZnO targets. In the small area system, RF sputtering is used, while in the in-line system, mid-frequency bipolar sputtering is used. Module encapsulation is accomplished using glass-glass vacuum lamination with EVA, with processing similar to that of the EPV-40 a-Si/a-Si module. For long-term outdoor testing, a Campbell Scientific datalogger is available.

2.0 Small Area CIGS Processing

2.1 Process recipes

R&D scale CIGS deposition is conducted in the Hercules 4-source system. This system is fitted with open boats for metal deposition and a baffled source for Se. It has been upgraded to accommodate six 5cm x 10cm stationary substrates per run rather than the four substrates previously accommodated. EPV has experimented with various recipes. Some of the more successful are:

a. Cu+Ga at T_1, In at T_1 - T_2, Cu+Ga at T_3 (evaporation)
b. Cu+Ga at T_1, In at T_1 - T_2, Ga at T_3 (evaporation)
c. Ga at T_1, In at T_1, Cu & ramp to T_2, In & Ga at T_2 (evaporation)
d. Ga at T_1, In at T_1, sputter Cu, selenize, In & Ga at T_2 (hybrid)

2.2 Boat material investigation

We have used molybdenum open boats with an alumina barrier as the evaporation source for Cu, In, and Ga in the Hercules system for a long time. However, the correlation between the Ga ratio Ga/(In+Ga) in the film as measured by ICP and the amount of Ga put in the boat for evaporation exhibited unexpected fluctuations. After observing Ga creeping on the boat surface as well as forming an alloy that remained in the boat, we investigated this issue carefully. We learned that Ga wets and alloys with molybdenum and tungsten, even though an alumina barrier helps minimize these effects. However, the alloying of Ga with tungsten is less severe than with molybdenum. A tungsten version of the boat was purchased and installed for Ga evaporation. There is now no evidence of Ga creeping either on the boat underside or on the alumina surface. There is also very little sign of Ga alloying with tungsten. The correlation mentioned above is now much more consistent and predictable.

2.3 Composition modeling

The geometrical configuration of the material sources and the substrate in the Hercules system is the following: the In boat is located in the center, while the Ga boat sits 2.5” left of center; substrate distance from the sources is 18”. We of course expect both In and Ga to have a gradient in the film. In order to get information about the composition distribution in the new hybrid process, composition modeling was established. In our normal process, we measure composition of the CIGS film after every run at four fixed locations by ICP. In Table I, we list the Cu and Ga ratios measured at these four locations for run H138, as well as the values calculated from our modeling. These results verify that our modeling works well. Therefore, we have confidence to believe the full composition distribution calculated from the modeling. For

example, the modeling predicts a variation of Ga ratio from 0.25 at the left edge (4" from the center) to 0.3 at the right edge (4" from the center) and Cu ratio from 0.73 in the center to 0.90 at upper right corner in our 8" x 8" substrate space for run H138.

Table I. Modeled versus measured Cu and Ga ratios for Hercules system

Sample ID and location	Cu Ratio		Ga Ratio	
	Measured	Modeled	Measured	Modeled
H138-1A	0.902	0.89	0.252	0.26
H138-1B	0.829	0.82	0.251	0.25
H138-6A	0.778	0.79	0.297	0.28
H138-6B	0.849	0.87	0.296	0.29

2.4 Study of indium gallium selenide layer

CIGS is often formed starting with an $(In,Ga)_2Se_3$ or In_2Se_3 first stage or precursor. The deposition conditions for this layer determine its composition, specularity, and crystal orientation, and these in turn can influence the subsequent CIGS growth and device performance. At low Se/In flux ratios (or at high T_s) the indium selenide film is (006)-oriented, rough, and InSe phases can appear (see Table II below). At higher Se/In ratios, the indium selenide film is (110)-oriented, specular, and is suitable for devices. Nothing is gained through use of even higher Se rates since the In_2Se_3 stoichiometry is self-regulating. Selenization of elemental indium represents Se-deficient growth and results in the (006) orientation [R4].

Table II. X-ray lines seen for In_2Se_3 (JCPDS file 40-1407) at small angles

Two theta (degrees)	Assignment		Strongest line seen for:
	In_2Se_3	other	
15.0489	(101)		
17.0037	(102)		
21.3414		(006) InSe*	
24.9670	**(110)**		**High Se/In ratio (normal co-evaporation)**
27.5864	(006)		Low Se/In ratio (and sequential)
28.2618		(13-1) Ga_2Se_3**	
28.5856	(113)		
29.2737	(201)		
30.3638	(202)		

*JCPDS 71-0447; **JCPDS 44-1012

A standard first stage layer was prepared in the Hercules system at 350°C on Mo-coated soda-lime glass (run H145A-6B). It consisted of Ga co-evaporated with Se followed by In co-evaporated with Se. The metal rates increased monotonically with time and then fell abruptly to zero as the source was exhausted. The film represented that used in devices in which 75% of the In and Ga were deposited in stage 1. Samples of this film were sent to NREL for analysis.

The XRD pattern for this film is shown below. The pattern matches In_2Se_3 and not $(In,Ga)_2Se_3$. It also appears that the (006) peak is comparable to the (110) peak. *This might indicate that the Se flux is inadequate during the time of highest In rate.*

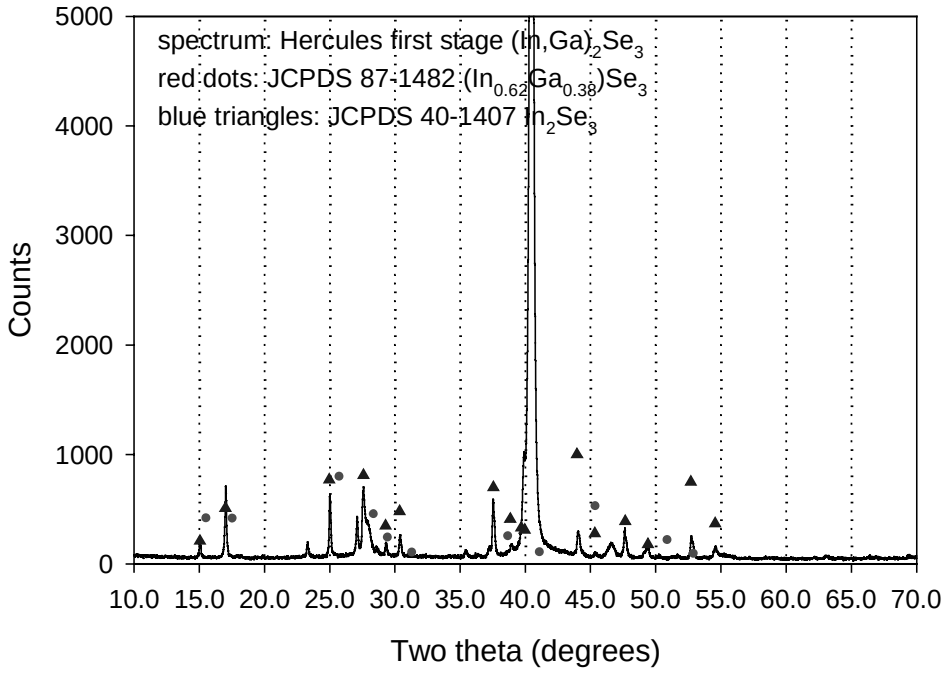

Fig. 1. XRD spectrum for Hercules first stage (In,Ga)Se

The film was also examined by SEM (see figures 2 and 3 below). The surface appeared specular. *The cross-section, however, clearly showed the layer to be stratified*, with a very fine grain layer adjacent to the (2-pass) Mo, and a much larger grain layer on top. The fine grain layer is presumably Ga_2Se_3 and the top layer In_2Se_3. The absence of Ga in this layer presumably makes it more difficult to obtain Ga in the bulk of the CIGS.

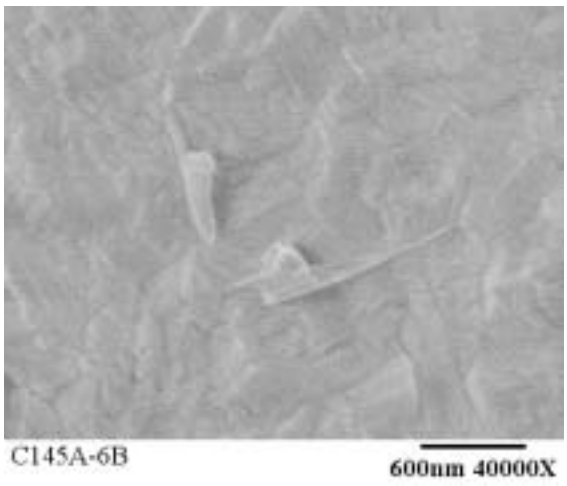

Fig. 2. SEM micrograph of the surface of a Hercules (In,Ga)Se film

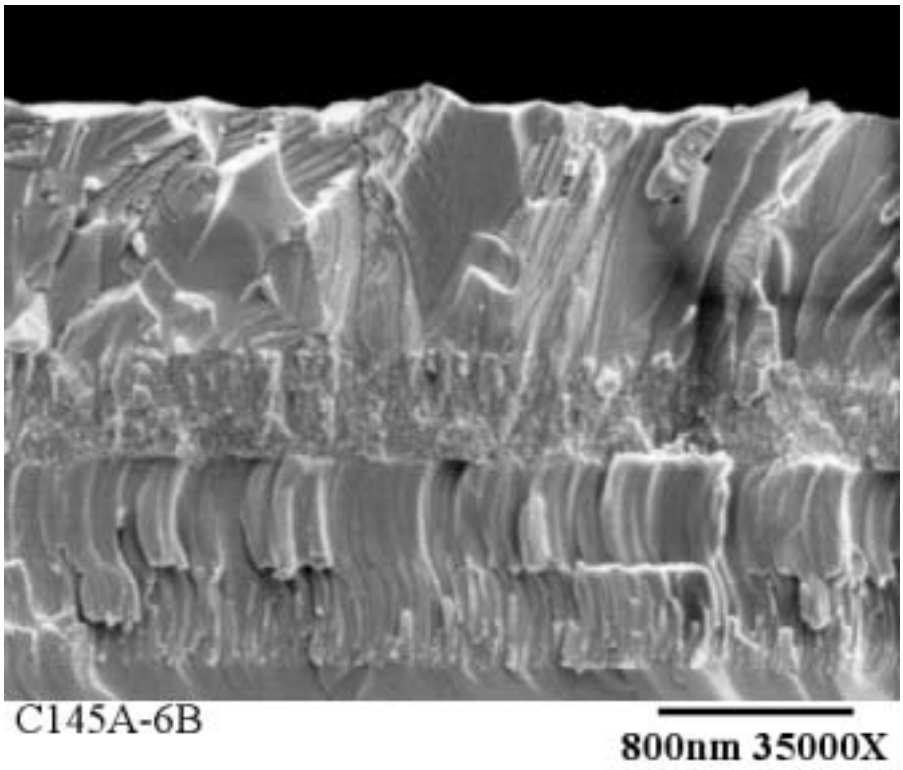

Fig. 3. Cross-section of a Hercules (In,Ga)Se film (on two-pass Mo) revealing the film to be stratified

Additional evidence that the stratification represents a compositional difference was obtained by EPMA analysis of the layer. At 20keV the apparent Ga/(Ga+In) atomic ratio was 9%, whereas at 10keV, which samples nearer the surface, the ratio was only 3.5% (In 40.3%, Ga 1.5%, Se 58.2%).

3.0 Large Area CIGS Processing

3.1 System capabilities, processing, and source height

Large area CIGS deposition is performed in the Zeus system using linear source evaporation onto moving substrates. A schematic diagram of part of the system is shown below in Fig. 4. [3]. As shown in the figure, the glass is transported on rollers, and the equipment is capable of heating the glass to the high temperatures necessary to produce device quality CIGS. The system is equipped with four downward-facing linear evaporation sources that may be used for Cu, In, Ga, and Se. The Zeus system has been shown capable of producing CIGS films with reasonably uniform thickness and composition, but, nevertheless, it was concluded that improvement of these parameters and of reproducibility would be necessary before module production could be undertaken with acceptable yield.

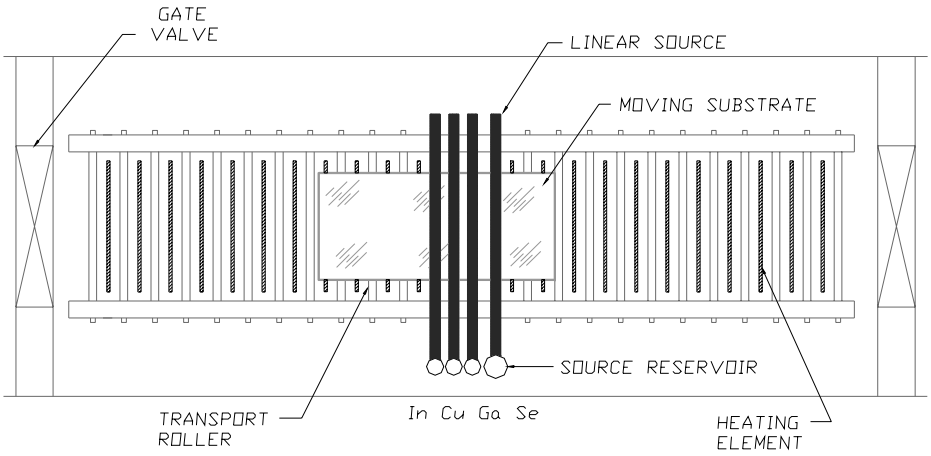

Fig. 4. Schematic of certain important elements of the Zeus deposition system for large area CIGS.

Following the recognition of these problems, we decided to explore a hybrid process designed to improve the uniformity of large area CIGS deposition. We had noticed for some time that the thickness uniformity of the evaporated Cu was less ideal than that of the In, Ga, or Se due mainly to its higher evaporation temperature (about 1300°C). In addition, we often observed spots on the film attributed to spitting from the Cu linear source. The hybrid process uses Cu sputtering to replace Cu evaporation. (We recognize that the sputtering rate may drift as the target is consumed, see for example [R5]). The process consists of the first stage In/Ga/Se evaporation (x %), Cu sputtering, and the final stage In/Ga/Se evaporation (1-x %) immediately after Cu selenization.

In parallel with these tests, we also raised the height of the In, Ga, and Se linear sources from the original 4" to diminish the peak heat flux from the linear sources to the substrate, since the oven temperature for In and Ga is around 1000°C while the substrate temperature is lower than 600°C.

The thickness distribution averaged over 18 hybrid process runs (obtained after raising of the sources), and measured along the linear source direction, is shown in Fig. 5. A modeling calculation for an evaporation-only process is plotted in the same figure as a comparison. The comparison clearly shows that uniformity is improved in our hybrid process. At the end of the second quarter, we were able to achieve a cell efficiency of 9.3 % in the large area Zeus system using the hybrid process. Contributing to the lower efficiency than observed in the Hercules system is a lower current density. The reason for this is being sought.

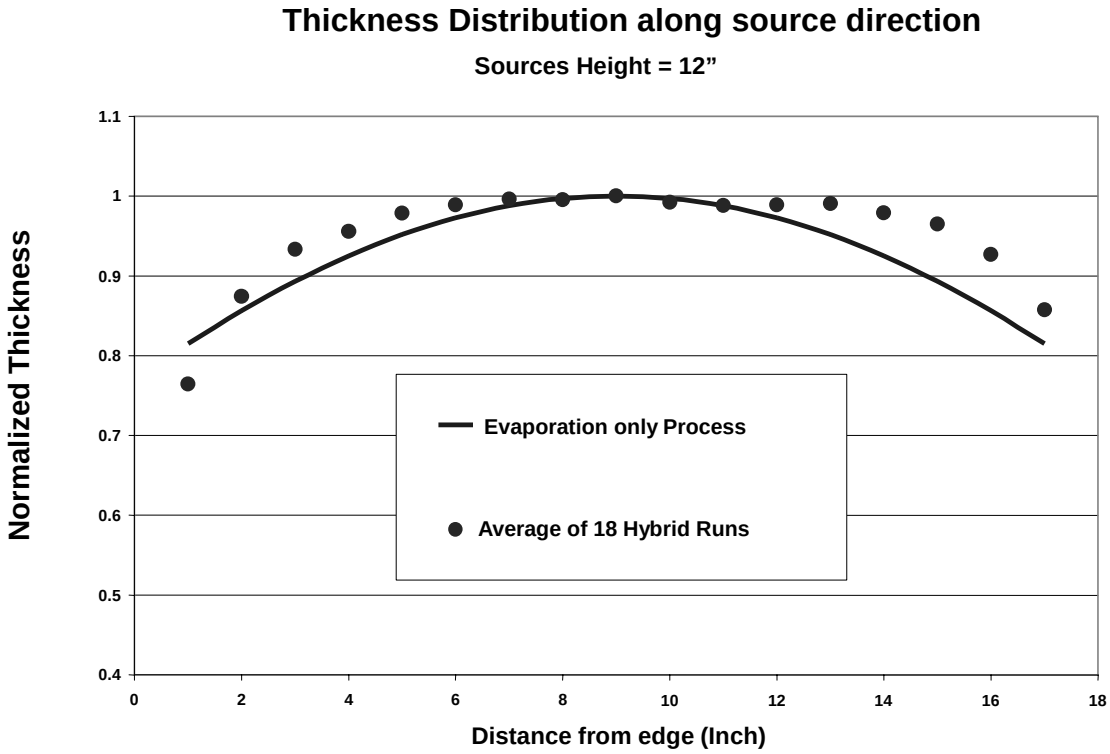

Fig. 5. **Thickness distribution averaged over 18 hybrid process runs**

We are also working on installing a Cu sputtering source in the entry/exit chamber of the Zeus system so that the entire IGS/Cu/IGS hybrid process can be finished without breaking vacuum.

3.2 Uniformity of thickness and composition for large area CIGS deposition

In our normal process for large area hybrid CIGS deposition in the Zeus, the thickness of both the sputtered Cu and the finished hybrid CIGS film are measured routinely along the linear source direction. The thickness uniformity achieved by sputtering Cu is excellent. A thickness distribution of 32 sputtered Cu runs averaged along the linear source direction is shown in Fig. 6. In our all-evaporation process, we normally have no way to know which sources are mostly responsible for non-uniformity in thickness and composition (Cu ratio and Ga ratio) of the CIGS film. However, we are now able to extract the information for each individual linear source in our hybrid process from composition measurement.

From Cu and Ga mole ratio definition:

$$\text{Cu ratio} = \text{Cu}/(\text{In}+\text{Ga}) \quad \text{(A)}$$

$$\text{Ga ratio} = \text{Ga}/(\text{In}+\text{Ga}) \quad \text{(B)}$$

We can easily solve for Ga/Cu and In/Cu ratio from equations (A) and (B)

$$(\text{Ga}/\text{Cu})\ \text{ratio} = \text{Ga ratio}/\ \text{Cu ratio} \quad \text{(C)}$$

$$(\text{In}/\text{Cu})\ \text{ratio} = 1/(\text{Cu ratio}) - (\text{Ga}/\text{Cu})\ \text{ratio} \quad \text{(D)}$$

By calculating (Ga/Cu) ratio and (In/Cu) ratio, we can now determine individual Ga and In distributions since Cu thickness is almost constant as seen in Fig. 6. For example, in Fig. 7, CIGS film thickness distribution of Zeus Run Z1542, we see a slight thickness non-uniformity near the plate edges, but we don't know which linear source (In or Ga) is responsible for it. By calculating (Ga/Cu) ratio (the 4th column) and (In/Cu) ratio (the 5th column) from Cu ratio (the 2nd col.) and Ga ratio (the 3rd col.) in Table III, it becomes transparent that the thickness non-uniformity in Run Z1504 results mainly from the In linear source.

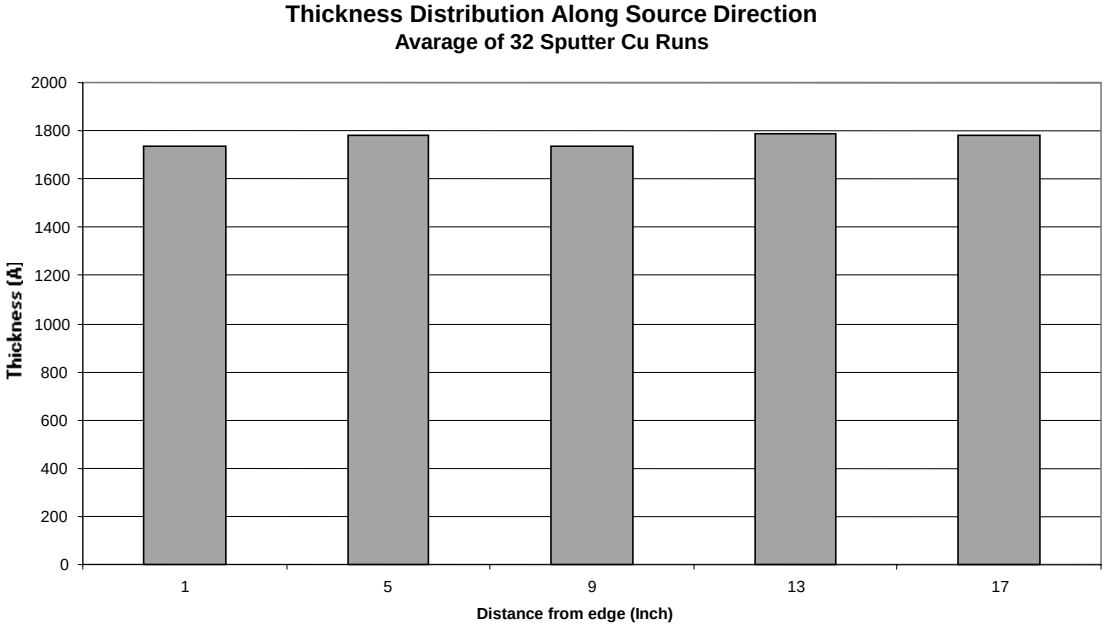

Fig. 6. Thickness distribution of sputtered Cu film along the source direction

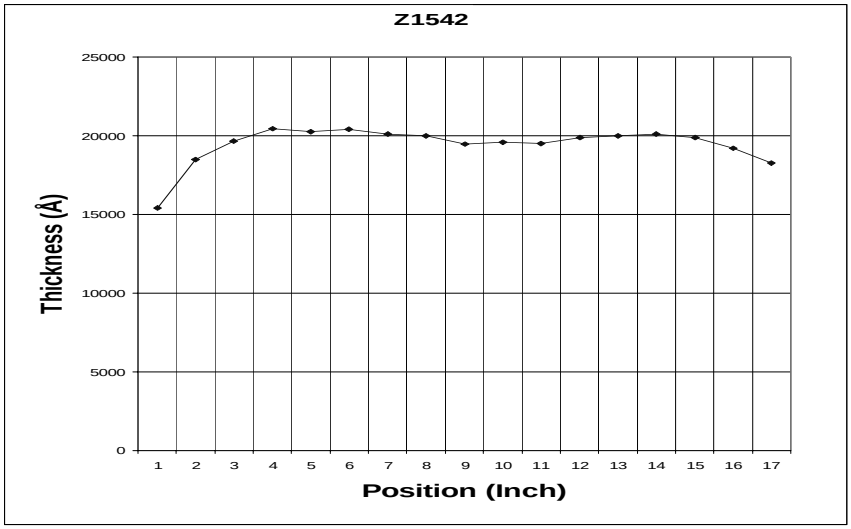

Fig. 7. Thickness distribution of CIGS film along the source direction in run Z1542

Table III. Composition in Run Z1542 along the source direction

Position (Inch)	Cu ratio Cu/(In+Ga)	Ga ratio Ga/(In+Ga)	(Ga/Cu) ratio	(In/Cu) ratio
3	0.92	0.31	0.33	0.75
7	0.87	0.28	0.32	0.83
11	0.84	0.27	0.32	0.86
15	0.95	0.30	0.32	0.74

We sometimes also evaluate stability of a linear source's effusion rate, plus constancy of temperature and translation speed of a substrate, by measuring composition along the direction of motion. In Fig. 8, such a composition distribution is plotted for Run Z1532.

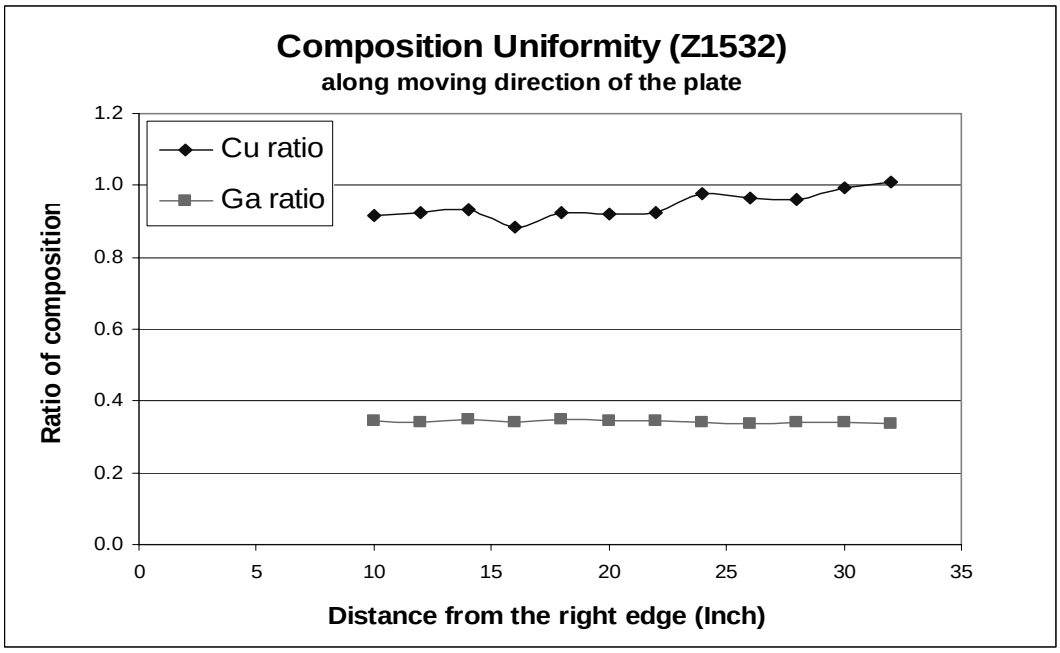

Fig. 8. Composition distribution in Run Z1532 along the direction of motion

3.3 Linear source uniformity (pressure modeling)

Two types of non-uniformity exist in our vapor delivery manifold:

- Edge effect due to geometry of linear source and substrate.
- Pressure effect due to gas flow along the manifold.

We have modeled and discussed the first type of geometrical non-uniformity on many occasions, see for example [3,4]. In this report, we focus on the second type of pressure non-uniformity.

In our Zeus system, vapor flows along a pipe from edge to center. Through many tiny holes in the pipe, vapor is delivered on a moving substrate. The pressure in the pipe, hence the vapor flow through the holes, is higher at the edge than that at the center. This pressure non-uniformity causes non-uniformity of effusion, which is what we are investigating.

We simplify the question as follows: There is only one open end in a pipe with eleven very tiny equally sized and spaced holes. Gas is injected into the open end of the pipe, and it is then delivered through these tiny holes. We would like to calculate the non-uniformity of the gas flow out of these tiny holes. The open end of the pipe is in the position of the first hole, and the closed end is that of the eleventh hole. The geometry of the pipe is such that l is the distance between two holes, D is the inner diameter of the pipe, while the geometry of the holes is such that d is the holes' diameter and t is the thickness of the pipe (see Fig. 9).

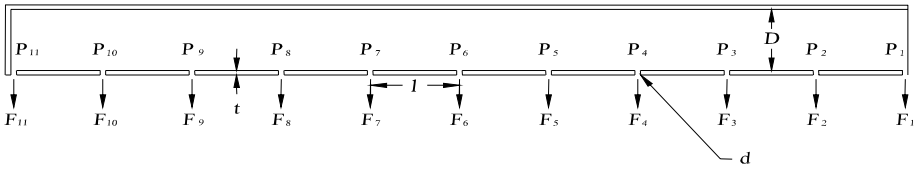

Fig. 9. Schematic and labeling for linear source

We call the gas pressure at the position of the first hole (at the inlet of pipe) P1, gas flow through the first hole F1, and so on. We have $P_i > P_{(i+1)}$ and $F_i > F_{(i+1)}$ with i=1,2,…,10. Total pressure non-uniformity is then defined as:

$$\Delta_{1\text{-}11} \equiv (F_1 - F_{11})/F_{11}$$

We call the gas conductance in a section of pipe between two holes C, and conductance of a hole α. Firstly, we calculate

$$\Delta_{10\text{-}11} \equiv (F_{10} - F_{11})/F_{11} = [(F_{10} - F_{11})/\alpha]/(F_{11}/\alpha)$$
$$= (F_{10}/\alpha - F_{11}/\alpha)/(F_{11}/\alpha) = (P_{10} - P_{11})/(F_{11}/\alpha) \quad (1)$$

The relationship among pressure, flow, and conductance is used in the last equation.
We also have

$$(P_{10} - P_{11}) = F_{11}/C \quad (2)$$

since flow from hole 10 to hole 11 is equal to the outlet flow through hole 11.
Having combined (1) and (2), we reach an extremely simple equation

$$\Delta_{10\text{-}11} = \alpha / C$$

We can write down an equation similar to (1),

$$\Delta_{9\text{-}10} \equiv (F_9 - F_{10})/F_{11} = [(F_9 - F_{10})/\alpha]/(F_{11}/\alpha) = (P_9 - P_{10})/(F_{11}/\alpha) \quad (3)$$

However,

$$(P_9\text{-}P_{10}) = (F11 + F10) / C \tag{4}$$

since the flow from hole 9 to hole 10 is equal to the sum of flows out of hole 11 and hole 10. Having combined (3) and (4), we reach another simple equation if we make the approximation F10 $\cong$ F11 by neglecting the second order difference

$$\Delta_{9\text{-}10} = 2 * (\alpha / C) \tag{5}$$

More generally we have

$$\Delta_{i\text{-}(i+1)} = (11\text{-}i) * (\alpha / C) \qquad i = 1, 2,\ldots 10 \tag{6}$$

Finally, we have the total pressure non-uniformity in the pipe with eleven holes

$$\Delta_{1\text{-}11} = \sum_{i=1}^{10} \Delta_{i\text{-}(i+1)} = (1+2+3+\ldots+10) * (\alpha / C) = 55* (\alpha / C) \tag{7}$$

The total pressure non-uniformity of the pipe with N holes will be

$$\Delta_{1\text{-}N} = \frac{N(N-1)}{2} * (\alpha / C) \tag{8}$$

if (α / C) is small.

It is crucial to find out what kind of flow regimes, such as viscous flow or Kundsen flow (molecular flow), exist in the pipe and in the hole by comparing the vapor mean free path λ with the dimension of the manifold. As the first step, we have to find the vapor pressure in the manifold. The 'average' pressure P in the pipe, after neglecting small non-uniform difference, is

$$P = F * (1/N\,\alpha) \tag{9}$$

where F is the total mass flow out of the N holes during deposition. It is about 0.0012 mole/minute at a deposition rate around 4 A/second in our large Zeus system. However, the formula to calculate hole's conductance α might depend on pressure P itself. Two types of formulae are applied at different flow regimes:

$$\alpha = \kappa \frac{\pi}{16} v d^2 \qquad \text{if } \lambda >> d \text{ and } t \qquad \text{in molecular regime} \tag{10a}$$

$$\alpha = \frac{\pi}{128\eta} \frac{d^4}{t} \overline{P} \qquad \text{if } \lambda << d \text{ and } t \qquad \text{in viscous regime} \tag{10b}$$

where η is the viscosity of vapor flow, v is the vapor thermal velocity, and $\overline{P}$ is the average pressure in the hole between pipe and vacuum, and it is about one half of average pressure P in the pipe. κ is a correction factor less than 1 for a non-ideal orifice with finite ratio of hole thickness t (pipe thickness in our case) to hole diameter d. The larger the ratio (t/d) is, the smaller κ is (κ = 1 at t/d = 0).

Since we don't know the type of regime in advance, we calculate both situations to see which one gives us a self-consistent solution.

Having combined (10a), (10b) with (9), we have

$$\overline{P} = \frac{8F}{N\pi\kappa v d^2} \tag{11a}$$

$$\overline{P} = \left(\frac{64\eta t F}{N\pi d^4}\right)^{0.5} \tag{11b}$$

Taking indium vapor at 1150 C as an example, we have

V = 510 m/s
η = 0.00076 poise

With t = d = 1.59 mm, κ = 0.514, N = 11, and F = 0.0012 mole/min., and we obtain the average pressure $\overline{P}$ in the hole,

$\overline{P}$ = 120 millitorr
$\overline{P}$ = 303 millitorr

The expression for mean free path is

$$\lambda = \frac{\kappa(T + 273)}{\sqrt{2}\pi\sigma^2(\overline{P}/760)} \tag{12}$$

Taking the collision diameter σ of indium to be 4 A, we have the numerical values

λ = 1.68 mm	under assumption λ >> d and t	(13a)
λ = 0.65 mm	under assumption λ << d and t	(13b)

Having compared the mean free path λ with the holes' size 1.59 mm, we conclude that an assumption of viscous flow through holes is a little better approximation than that of molecular flow, although neither is great. Hereafter, we make the viscous flow approximation in the hole in our calculation. For the vapor flow in the pipe, the average pressure is about two times the average pressure in the hole, and thus viscous flow is a very good approximation because λ (0.33 mm) is much less than pipe dimension D 22.2 mm.

We can easily obtain the ratio of a hole's conductance α to a section of pipe conductance C since both follow the same formula (10b)

$$(\alpha / C) = \frac{1}{2}\left(\frac{l}{t}\right)\left(\frac{d}{D}\right)^4 \tag{14}$$

and the total pressure non-uniformity of the pipe with N holes

$$\Delta_{1\text{-}N} = \frac{N}{4}\left(\frac{L}{t}\right)\left(\frac{d}{D}\right)^4 \tag{15}$$

where L is total length of pipe with L = $(N-1)l$. For $d = t$ = 1.59 mm, D = 22.2 mm, L = 254mm, and N = 11, we finally have the pressure non-uniformity in our Zeus system

$$\Delta_{1\text{-}11} = 1.2\ \%$$

It is clear from (15) that the pressure uniformity can be further improved by

1. Increase of pipe inner diameter *D*.
2. Reduction of hole diameter *d*.
3. Increase of pipe thickness *t*.
4. Reduction of hole's number *N*.

It should be noted that the trend of geometrical non-uniformity is opposite to that of pressure non-uniformity. The former leads to deposition being thinner near the edges, while the latter, as we mentioned earlier, yields deposition thicker near the edges. Therefore, the two factors tend to cancel each other, so that the total non-uniformity is somehow improved although geometrical non-uniformity is still a dominant factor (about 15%).

In our next generation system, the substrate plate width will increase to 25 inches from 17.5 inches. The pressure non-uniformity will increase roughly following the square of the width. From (15) that yields the pressure non-uniformity to be

$$\Delta_{1\text{-}N} = 2.4\%$$

which is still much smaller than geometrical non-uniformity**.**

3.4 Impurities in CIGS: the case of Zn

From SIMS analyses of Hercules CIGS films (performed by Sally Asher at NREL) we had noticed the apparent presence of various metallic impurities, including Al, Fe, Zn, and Ni, and also C. It occurred to us to investigate whether some of these elements might be quantifiable using our in-house ICP atomic emission spectrometer. Unfortunately, interference effects ruled out detection of carbon. Next, attention was turned to zinc, since as a group II element it might act as an n-type dopant in CIGS. As the base CIGS is supposed to be p-type, doping with Zn might very well compensate the material and result in lower V_{oc}. And as V_{oc}'s over 600mV have rarely been achieved at EPV, persistent Zn contamination could conceivably be a contributing factor.

A review of emission lines revealed a good chance that zinc could be detected. We found that In, Ga and Se do not interfere with Zn, while almost all of the atomic emission lines of Zn are interfered by Cu. After carefully checking the Zn lines, we decided to take the Zn <u>213.856</u> nm line as our analytical line because

1. It has high intensity (1020), which is needed for detecting a tiny amount of Zn in a CIGS film.

2. It is in the third order spectrum from the monochromator, meaning it has a narrower bandwidth, and high resolution to avoid or reduce interference.

There are two Cu lines 213.598 nm (intensity 120) and 213.853 nm (intensity 4.5) very close to it. Since the amount of Cu in a CIGS layer is much greater than that of Zn, the Cu lines might boost the Zn signal at <u>213.856</u> nm. In order to see how large this effect is, we designed the

following experiment. We used a ***Standard Zn*** solution (100 ppm for Cu, In, Ga, Se, and Zn) as the test standard and used a ***Standard 100*** solution (100 ppm for Cu, In, Ga and Se) as an unknown. The test result is listed in Table IV below:

Table IV. ICP measurement of non-zinc-containing solution

Element	As made (ppm)	As measured (ppm)	After correction
Cu	100	99.2	
Ga	100	100.4	
In	100	99.2	
Se	100	99.7	
Zn	0	0.24	0 = 0.24-0.24

As shown in the table, we have a reading of 0.24 ppm for Zn in a solution that does not contain Zn. It presumably comes from Cu interference on Zn. The ratio 0.0024 (0.24 ppm Zn/100 ppm Cu) gives the error from interference. So we correct this error by setting

Corrected Zn amount = Measured Zn amount – Measured Cu amount* 0.0024 [16]

We also conclude that interference from Zn on Cu in the standard is minor, because the measured Cu number (99.2 ppm) is very close to the true number (100 ppm). This conclusion allows us to use the new ***Standard Zn*** solution to replace old ***Standard 100*** solution. Furthermore, it is verified by measuring several samples with the two different standard solutions. The results are shown in Table V below.

Table V. ICP measurement of CIGS samples using two different standard solutions

Sample	Cu / (In+Ga)		Ga / (In+Ga)	
	Normal stand.	Zn stand.	Normal stand.	Zn stand.
H108-1AI	0.72	0.73	0.28	0.27
H108-1BI	0.73	0.74	0.28	0.28
H108-6AI	0.64	0.65	0.25	0.26
H108-6BI	0.64	0.66	0.26	0.25

In two early samples (H107-1B and H107-6A) that were examined, a considerably larger amount of Zn than the interference background from Cu was detected, while later samples from the Hercules system showed only the background level. We will resume impurity testing for Zn in the next quarter.

4.0 Post-deposition Treatment (CIGS)

4.1 Initial studies

Usually we find that module and cell performance deteriorates if, after CIGS deposition, the CdS deposition is delayed. Many ways to clean the CIGS surface were tried during the second quarter. We cut a series of 1” x 2” samples from a large CIGS plate (made in the Zeus) along the direction of glass travel to ensure the best possible uniformity. First, several different solutions were chosen to screen for better detergents. The test result is listed in Table VI. In each 1” x 2”

sample, 32 cells were cut and defined. We call a cell bad if its leakage current is larger than 1% of short-circuit current.

Table VI. Results of cleaning CIGS

ID	Detergent	CdS	Voc	FF	Jsc(QE)	Efficiency	# bad
Z1493A	No	CBD	455.4	44.63	21.36	4.34	11
Z1493B	No	CBD	449	40.37	22.11	4.01	3
Z1493E	Acetic acid	CBD	441.4	45.12	24.43	4.87	2
Z1493F	Acetic acid	CBD	429.5	35.09	21.59	3.25	5
Z1493I	Water, soap	CBD	415.6	29.98	17.95	2.24	8
Z1493J	Water, soap	CBD	CIGS peeled off all samples in this group				
Z1493M	FeCl3	CBD	539.2	40.94	18.64	4.11	1
Z1493N	FeCl3	CBD	530	44.81	17.68	4.20	0

Table VI clearly shows that use of FeCl3 to 'clean' the CIGS surface drastically increases Voc, reduces the number of bad cells (i.e. partially eliminates cell shunting), but results in reduced J_{sc}.

Second, additional solutions with different concentrations, temperature and treatment time were tested. The results are shown in Table VII. Comparing with the control cell, we find that solution Y yields the best results. All four parameters (Voc, FF, Jsc and bad cell #) are improved. We subsequently repeated tests with treatment Y a couple of dozen times, and overwhelming evidence convinces us of its effectiveness. Even more encouraging, we found in most cases that cell performance not only recovers from the aging effect due to delayed CdS deposition, but also that the performance is superior to its fresh CIGS peer.

Table VII. Results of further CIGS treatment experiments

ID	Solution	Voc	FF	Jsc(QE)	Efficiency	# bad	M	Temp.	Time
Z1492	Control	457.3	54.4	20.4	5.08	27(27)			
Z1492B	Y	521.5	54.3	26.7	7.57	2(36)			
Z1492C	Y	544.8	60.0	23.6	7.72	2(36)			
Z1492E	HCl	436.0	47.3	18.7	3.86	1(36)	1%	26C	120 min.
Z1492H	HCl	428.2	47.1	19.4	3.92	5(36)	1%	26C	120 min.
Z1492F	FeCl3 diluted	511.8	40.3	19.9	4.10	10(36)	10%	26C	30 sec.
Z1492I	FeCl3 diluted	393.5	47.6	17.3	3.25	10(36)	10%	26C	60 sec.
Z1492G	Na2(SO4)2	520.8	41.2	20.8	4.45	6(36)	0.25M	40C	60 sec.
Z1492K	Na2(SO4)2	402.5	46.6	20.5	3.84	9(36)	0.25M	40C	60 sec.

Finally, we use DOE (design of experiment) to optimize Y treatment conditions. Eight samples were treated with a full factorial design of three process variables (temperature, concentration and time, with two levels each. The design and the results are listed in Table VIII.

Table VIII. Optimization of treatment Y using design of experiment approach

ID	Temperature	Concentration	Time	Voc	FF	Jsc	Efficiency
Z1504A	High	Low	High	505.8	61.61	25.19	7.85
Z1504B	High	High	High	530.1	66.7	24.59	8.69
Z1504C	High	High	Low	513.3	64.62	25.02	8.3

Z1504D	Low	High	High	534.3	66.84	25.06	8.95
Z1504F	Low	Low	High	507.3	64.19	24.49	7.97
Z1504G	Low	High	Low	517.1	62.24	25.07	8.07
Z1504H	High	Low	Low	500	61.74	25.53	7.88
Z1504-I	Low	Low	Low	497	60.25	25.09	7.51

Statistical methods are used to analyze the data and to find correlations between cell performance and process variables. A detailed statistical and graphic analysis was performed.

The main conclusions include:

- Voc shows strongly positive correlation (the higher level of process variable is, the better performance) with concentration, and also shows a moderate positive correlation with time, while it has no statistically significant correlation with temperature in the range of experiment.
- FF shows strongly positive correlation with both time and concentration while it has no statistically significant correlation with temperature in the range of experiment.
- Jsc shows no clear correlation with concentration, temperature or time.

The results indicated we needed to increase concentration and time further in the second round DOE while keeping temperature unchanged. After several DOE steps we reached a saturation point beyond which cell performance did not show improvement upon increase of concentration or time. We notice Voc and FF increase with CIGS treatment time, which might imply that the effect of treatment is not only to clean the surface, but to change bulk properties as well.

4.2 Universality of results

In our last quarterly report, we reported our very promising finding of post-CIGS deposition treatment. More comparison experiments were conducted in this quarter. We are focusing on answering two main questions:

- Is the cell performance improvement sample-independent?
- Is the cell performance improvement CdS-deposition-independent?

To answer the first question, we took samples made in two different systems, namely Zeus and Hercules, for the post CIGS treatment. The results are shown in Table IX.

Table IX. Post-treatment samples from Z and H systems

ID	Post-treatment	CIGS made in	Voc	FF	Jsc(QE)	Efficiency
Z1504-AA	**Yes**	**Zeus**	**542.8**	**66.81**	**24.12**	**8.75**
Z1504-BB	**Yes**	**Zeus**	**546**	**68.68**	**24.49**	**9.18**
Z1504-CC	**Yes**	**Zeus**	**546.8**	**67.38**	**23.44**	**8.64**
Z1504-DD	**Yes**	**Zeus**	**551**	**67.07**	**24.41**	**9.02**
Z1504-EE	No	Zeus	370.4	50.19	21.61	4.02
Z1504-KK	No	Zeus	405.8	53.44	22.73	4.93
H150-5AB4	**Yes**	**Hercules**	**546.6**	**69.70**	**28.77**	**10.96**
H150-5BB6	No	Hercules	513.3	49.73	27.32	6.97

H150-3DD3	**Yes**	**Hercules**	**525.8**	**64.24**	**29.59**	**10.00**
H139-4 B	No	Hercules	538.7	46.92	27.56	6.97

To answer the second question, we used two different CdS deposition recipes after the post-CIGS treatment. The results are shown in Table X.

Table X. Post-treatment with two different CdS recipes

ID	Post-treatment	CdS	Voc	FF	Jsc	Efficiency
Z1504-3	No	Recipe 1	397.8	33.19	23.67	3.13
Z1504-8	**Yes**	**Recipe 1**	**482**	**59.19**	**25.74**	**7.34**
Z1504-10	**Yes**	**Recipe 1**	**481.7**	**58.17**	**26.22**	**7.35**
Z1504-12	No	Recipe 1	382.6	41.62	23.93	3.81
Z1504-4	**Yes**	**Recipe 2**	**507.5**	**60.58**	**26.25**	**8.07**
Z1504-7	No	Recipe 2	442.8	55.13	24.51	5.98
Z1504-9	**Yes**	**Recipe 2**	**520.4**	**62.55**	**25.74**	**8.38**
Z1504-13	No	Recipe 2	435.2	35.83	19.75	3.08

Both results clearly show that our post-CIGS treatment is successful and effective in all experimental cases. It seems to be a "universal" improvement in EPV internal samples. We are contacting other organizations such as NREL and Uppsala University in Sweden to obtain their CIGS films, and are eagerly hoping to further verify its universality. At EPV, we have already adopted this treatment as a standard process step.

4.3 Materials characterization before and after treatment

We have reported the effectiveness of our post-CIGS treatment in quarterly reports in detail. A dramatic increase of device V_{oc} and FF after post treatment is observed in almost all comparison tests of EPV CIGS samples. To understand better the link between device performance and materials properties of the absorber layer, we continued studying the material characterization in house as well as in collaboration with some other institutions.

Some characterizations as well as main results are listed below:

1. Surface properties
    a) Surface reflectivity: Absorber layer reflectivity in visible range after treatment is reduced.
    b) SEM pictures show no noticeable difference between treated and non-treated.

2. Electrical properties
    a) Lateral conductivity measured directly on CIGS film increases after treatment.
    b) The slope of (A^2/C^2) vs. voltage of CIGS devices after treatment decreases, which indicates increasing doping density.
    c) Hall Effect measurement done at University of Florida by Prof. Li's group shows that lateral conductivity increase while mobility decreases after treatment. Their results are listed in Table XI.

Table XI. Hall effect results for EPV CIGS samples

Sample Number	**H152-4A**	**H152-4B**
Resistivity (Ω*cm)	284	189.1
Mobility (cm2/Vs)	164.4	20.8
Density (cm-3)	$1.336*10^{14}$	$1.587*10^{15}$
Hall Coeff. (cm3/C.)	$4.673*10^{4}$	$3.934*10^{3}$
Sheet Number (cm-2)	$2.672*10^{10}$	$3.173*10^{11}$
Sheet Resistance (Ω/square)	$1.42*10^{6}$	$9.457*10^{5}$
Type of Carriers	Holes	Holes
EPV Treatment	Untreated	Treated

Here are some comments regarding the electrical properties measurement. Both 2a) and 2c) show that lateral conductivity after treatment increases, and Hall effect further indicates increase of conductivity is due to increase of carrier density rather than mobility. The assertion is exactly what we found from 2b) C-V measurement, although ratio increase (a factor of 4) appears smaller in C-V measurement than in Hall measurement (a factor of 10). Increase of carrier density could explain increase of Voc as it would reduce depletion width; this might cause FF to drop, contrary to what we observed. In addition, CIGS devices operate in a direction perpendicular to the film, therefore the reduced lateral mobility observed by the Hall effect might not be relevant to cell performance.

3. Composition

   a) Cu ratio and Ga ratio measured by ICP-AES show no bulk composition difference before and after treatment.
   b) Element depth profile measured with SIMS at University of Illinois by Prof. Rockett's group. (We could observe some difference between treated H150-3D and untreated H150-3C.)

5.0 Junction Formation

5.1 Investigation and optimization of CBD CdS process

CdS deposition plays a far more vital role in the performance of CIGS devices than what we previously thought. Four parameters, namely Cd and S source material, concentration, temperature, and process time, are the main variables in the process optimization.

Table XII. Process comparison of CBD CdS

Groups	C (M) Thiourea For S	C (M) Cd Acetate	C (M) Cd Sulfate	Ratio (S/Cd)	Ammonium hydroxide (M)	Process temperature	Process time
EPV*	0.017	0.0017		10	2.5	77 C	14 min.
NREL	0.075		0.0015	50	2.0	65 C	13 min.
IEC	0.15		0.0015	100	2.0	40-70 C	5 min.

* prior to this optimization

Having compared the CBD CdS process in NREL and IEC with EPV (see Table XII above), we found the differences among the organizations to be quite significant.

To obtain the optimum recipe for our CIGS films produced in both Zeus and Hercules systems, a set of designed experiments was set up. The test results and its conditions are listed in Table XIII.

Table XIII. CBD CdS optimization

Sample ID	**Cd source**	**(S/Cd) ratio**	**Temp. range** C	**Time** (min.)	**Voc** (mV)	**FF**	**Jsc(0)** (mA/cm2)	**Eff.** (%)	Comments
Z1532I	Acetate	10	62-66	13.0	461	54.3	27.5	6.88	
Z1532A	**Acetate**	**10**	**63-65**	**30.0**	**423**	**52.3**	**31.2**	**7.11**	
Z1532B	Acetate	10	71-75	7.5	447	49.5	30.1	6.67	
Z1532J	Acetate	50	61-65	5.5	531	48.1	24.1	6.16	
Z1532C	Acetate	50	61-65	4.5	565	44.9	23.9	6.08	
Z1532D	Acetate	50	70-75	3.0	519	44.7	25.9	6.00	
Z1532F	Sulfate	50	55-64	13.4	536	47.6	22.9	5.84	
Z1532K	Sulfate	50	61-65	7.0	536	45.3	27.0	6.56	
Z1532E	Sulfate	50	65-68	5.0	518	47.5	25.8	6.33	
Z1532G	**Sulfate**	**100**	**55-60**	**6.0**	**526**	**54.3**	**25.9**	**7.39**	
Z1532L	Sulfate	100	59-64	5.0	554	41.2	23.3	5.32	Collection problem
Z1532H	**Sulfate**	**100**	**64-67**	**3.2**	**558**	**56.2**	**24.1**	**7.55**	
H145-I	Acetate	10	62-66	13.0	452	57.6	31.6	8.23	
H145-A	Acetate	10	63-65	30.0	435	50.2	27.4	5.98	
H145-B	Acetate	10	71-75	7.5	465	62.7	29.7	8.65	
H145-J	Acetate	50	61-65	5.5	459	59.3	30.4	8.26	
H145-C	Acetate	50	61-65	4.5	522	65.3	29.3	9.97	
H145-D	Acetate	50	70-75	3.0	489	69.0	28.4	9.61	
H145-F	Sulfate	50	55-64	13.4	467	57.4	28.8	7.73	
H145-K	Sulfate	50	61-65	7.0	480	51.9	29.0	7.23	
H145-E	**Sulfate**	**50**	**65-68**	**5.0**	**519**	**64.5**	**30.1**	**10.07**	
H145-G	**Sulfate**	**100**	**55-60**	**6.0**	**519**	**66.1**	**29.4**	**10.06**	
H145-L	Sulfate	100	59-64	5.0	519	55.4	31.4	9.02	shunting
H145-H	**Sulfate**	**100**	**64-67**	**3.2**	**501**	**70.3**	**29.6**	**10.43**	

It is clear from the data of Table XIII that most of the highest performance devices result from the following conditions:

- Using Cd sulfate as the Cd source.
- With a higher S/Cd ratio near 100.
- At not too high process temperature: 55C-68C.

These parameters are effective for CIGS films made from both Zeus and Hercules (the basic CIGS process are the same), which means that the best CBD CdS recipe in our case is system-

independent. By the way, these conditions are actually very close to the conditions used in IEC. Since then, we settled our new standard CBD CdS deposition to be close to these conditions.

5.2 Development of spray CdS

Table XIV shown below summarizes the results obtained from a study involving sprayed CdS for junction formation.

Table XIV. Early device results obtained with sprayed CdS

Sample ID	Position	Voc	FF	Jsc from QE	Eff	Tem.	Surf. treat	Conc.	Surfact
Z1487A					0.00	90	No	0.01M	
Z1487B	C3	275.6	31.02	16.97	1.45	90	Yes	0.01M	
Z1487C					0.00	90	No	0.1M	
Z1487D					0.00	90	Yes	0.1M	
Z1487E	A1	443.8	41.28	25.34	4.64	90	No	0.05M	
Z1487F					0.00	90	Yes	0.05M	
Z1487G	A1	410.3	44.99	24.44	4.51	90	No	0.025M	
Z1487H	A1	504.2	51.15	21.92	5.65	90	Yes	0.025M	
Z1495 I	B5	383.4	37.67	21.69	3.13	90	No	0.01M	Alcohol
Z1496 J	A1	403.1	37.74	20.72	3.15	90	Yes	0.01M	Alcohol
Z1487K	C4	382.5	33.61	21.58	2.77	90	No	0.01M	Alcohol
Z1487L	C5	186.6	30.34	18.58	1.05	90	Yes	0.01M	Alcohol

Development of an in-line CdS spray process would have several merits:

- Environmental friendliness due to its very high Cd utilization.
- Reduced delay time between CIGS and CdS.
- High speed.
- Enables all deposition processes in module production to be in-line.

We have done some further experiments to deposit spray CdS film. CdS films were deposited on both plain glass and CIGS samples. Those on glass are used for measuring optical transmission to compare the films' thickness with those from CBD CdS. The process variables are: chemicals and their concentration, substrate temperature, spray pressure, and spray height. We found substrate temperature is the most crucial variable. It controls the speed of chemical reactions and thus the film properties. It only works in a narrow window around 90°C – 130°C. We have been able to deposit nice-looking, uniform films with thickness comparable to those from CBD. Devices with spray CdS have been processed, and some show promising results. In Table XV, a set of spray CdS devices and their performance are listed. The best efficiency is 5.65 %, which, in this case, is better than that from CBD CdS.

Table XV. Further device results with sprayed CdS

Sample ID	Position	Voc	FF	Jsc QE	Efficiency	Temp	Surface treatment	Conc.
Z1487A	A1	384.5	43.11	24.13	4.00	90	No	0.01M
Z1487B	C3	275.6	31.02	16.97	1.45	90	Yes	0.01M
Z1487C	A1	383.3	34.06	19.51	2.55	90	No	0.1M
Z1487D	A1	488.9	27.14	13.28	1.76	90	Yes	0.1M
Z1487E	A1	443.8	41.28	25.34	4.64	90	No	0.05M
Z1487F	C5	393.8	35.29	25	3.47	90	Yes	0.05M
Z1487G	A1	410.3	44.99	24.44	4.51	90	No	0.025M
Z1487H	A1	504.2	51.15	21.92	5.65	90	Yes	0.025M
Z1487 I	B5	383.4	37.67	21.69	3.13	90	No	0.01M
Z1487 J	A1	403.1	37.74	20.72	3.15	90	Yes	0.01M
Z1487K	C4	382.5	33.61	21.58	2.77	90	No	0.01M
Z1487L	C5	186.6	30.34	18.58	1.05	90	Yes	0.01M

Sprayed CdS, ZnS, and In_2S_3 Films

We continued our work on spray deposition with the thin films ZnS and In_2S_3. Based on the apparent advantages of the spray pyrolysis technique, such films, either used alone or in conjunction with each other, are expected to be part of a future in-line CIGS production process.

We have deposited ZnS and In_2S_3 thin film on plain glass as well as on CIGS. We are optimizing the deposition parameters, namely, spray solution concentration and composition, and deposition temperature (in the range of 90C-130C). This low deposition temperature is the most encouraging factor for in-line production. We are also optimizing the spray inert gas pressure, and the distance between the nozzle and substrate. Thus far we have been able to deposit very uniform and quite transparent films for all of these films. Some preliminary work on devices has been done, and efficiencies of about 4% were reached.

5.3 Dry processing: zinc indium selenide and other novel buffer layers

We continue to aggressively pursue $ZnIn_2Se_4$ (ZIS) as a buffer material [5]. Some of this work is described in our paper presented at the 29th IEEE PVSC [6] (copy reprinted after Section 8.0, Phase I Summary). This paper describes a 10.1% ZIS cell on EPV CIGS (503mV, 29.7mA/cm^2, FF 67.4%), with In_2S_3 being found to be decidedly inferior, and ZnSe being found to be a useful buffer material but still inferior to ZIS.

At the time of writing this PVSC paper, ZIS achieved almost 90% of the performance of CBD CdS. Subsequently, however, one of the post-deposition treatments of CIGS described in Section 4 was found to clearly improve cells with CBD CdS but not cells with ZIS, thereby allowing CBD CdS to pull ahead again. Thus within the ZIS program, 11.6% and 12.1% control cells were made with surface-treated CIGS/CBD CdS (554mV, 30.1mA/cm^2, FF 69.7% and 528mV, 34.5mA/cm^2, FF 66.3%).

We continued to explore alternative junction formation methods focusing mostly on ZIS, with parallel work on CBD CdS as a reference. Some of the summary tables for experiments conducted in the third quarter are reproduced in Table XVI below.

Table XVI. Summary tables for inter-comparison of various buffer layers, including ZIS

Series A: CIGS treatment prior to ZIS									
	BEST DEVICES				*AVERAGE VALUES*				Av. Voc
	Voc	*Jsc*	*FF*	*η*	*Voc*	*Jsc*	*FF*	*η*	all cells
163-A-D3- - H135-4/n w/ZIS+ZnSe	*429*	*28*	*46.3*	*5.55*	*405.9*	*28*	*41.3*	*4.69*	*410.25*
163-B-B1 - H135-4/wd/ZIS+ZnSe	*469*	*30.8*	*57.1*	*8.24*	*468.6*	*30.8*	*55.7*	*8.02*	*465*
165-B3 - H135-4/treat/ZIS+ZnSe	*450*	*29.4*	*58*	*7.68*	*435.3*	*29.4*	*50.6*	*6.48*	*425.81*
166-D1 - H135-4/wd/ZnSe	*465*	*28.7*	*60.3*	*8.04*	*455.5*	*28.7*	*59.8*	*7.82*	*458.87*

Series B: CIGS treatment prior to CdS									
	BEST DEVICES				*AVERAGE VALUES*				Av. Voc
	Voc	*Jsc*	*FF*	*η*	*Voc*	*Jsc*	*FF*	*η*	all cells
CdS-1-A2 - H139-4/no treat/CdS	*391*	*27.8*	*49.5*	*5.38*	*380.7*	*27.8*	*49*	*5.19*	*359.18*
CdS-2-D3 - H139-4/treat/CdS	*493*	*33.2*	*63.9*	*10.43*	*493.3*	*33.2*	*63.1*	*10.32*	*473*

Series C: CBD CdS optimization									
	BEST DEVICES				*AVERAGE VALUES*				Av. Voc
	Voc	*Jsc*	*FF*	*η*	*Voc*	*Jsc*	*FF*	*η*	all cells
A1-A1 - H139-4/treat/CdS-75-S/Cd=10,nZnO	*486*	*35.3*	*63.3*	*10.85*	*478.8*	*35.3*	*59.6*	*10.07*	*485.18*
A2-C1 - H139-4/treat/CdS-75-S/Cd=75,nZnO	*534*	*30.7*	*66.7*	*10.92*	*541.2*	*30.7*	*64.3*	*10.66*	*498.93*
A3-B1 - H139-4/treat/CdS-75-S/Cd=75,i+nZnO	*528*	*34.5*	*66.3*	*12.06*	*529*	*34.5*	*63.6*	*11.60*	*531.68*

Series D: CIGS treatment prior to ZIS & CdS									
	BEST DEVICES				*AVERAGE VALUES*				Av. Voc
	Voc	*Jsc*	*FF*	*η*	*Voc*	*Jsc*	*FF*	*η*	all cells
171-A-A2 - H141-4/treat/ZIS+S/ZnSe	*281*	*27.9*	*31.3*	*2.46*	*261.4*	*27.9*	*30*	*2.19*	*230.22*
171-B-A2 - H144-4/wd/ZIS+S/ZnSe	*396*	*28*	*41.7*	*4.61*	*376.2*	*28*	*37.7*	*3.96*	*324.93*
CdS144-A1 - H144-4/treat/CdS-75-S/Cd=75	*451*	*31.5*	*60*	*8.52*	*452*	*31.5*	*59.2*	*8.42*	*439.35*

Series E:Buffer combinations									
	BEST DEVICES				*AVERAGE VALUES*				Av. Voc
	Voc	*Jsc*	*FF*	*η*	*Voc*	*Jsc*	*FF*	*η*	all cells
072902-1A-C2 H144-2/wd/ZIS/ZnSe	*416*	*28.6*	*23.5*	*2.79*	*417.7*	*28.6*	*22.8*	*2.72*	*386*
072902-2A-A4 H144-2/wd/ZIS/treat/ZnSe	*496*	*32.5*	*60.8*	*9.79*	*496.2*	*32.5*	*58.6*	*9.45*	*473.12*
072902-3A-A2 H144-2/wd/ZIS(15)/CdS	*473*	*31*	*59.1*	*8.66*	*462.8*	*31*	*58.6*	*8.39*	*413.56*
072902-4A-D3 H144-2/treat/CdS	*497*	*27.5*	*65.2*	*8.93*	*501.2*	*27.5*	*62.3*	*8.60*	*476.78*
072902-5A-C3 H144-2wd/ZIS(15)/CdS	*477*	*32.5*	*65.5*	*10.14*	*473.8*	*32.5*	*62.6*	*9.63*	*438.93*
072902-6A-C1 H144-2/wd/ZIS(25)/CdS	*448*	*31.2*	*62.2*	*8.68*	*444.3*	*31.2*	*60.3*	*8.34*	*423.31*
072902-7A-B1 H144-2/treat/ZIS/ZnSe	*414*	*29.5*	*60.3*	*7.37*	*411.8*	*29.5*	*59.8*	*7.26*	*388.93*

Series F: ZIS and buffer-free device									
	BEST DEVICES				*AVERAGE VALUES*				Av. Voc

	Voc	Jsc	FF	η	Voc	Jsc	FF	η	all cells
080902-1-A4 - H146-3/hw(85C)/ZIS/ZnSe	*409*	*28.6*	*44.4*	*5.19*	*375.1*	*28.6*	*38.3*	*4.10*	*293*
080902-2-D4 - H144-4/treat/ZIS+S/ZnSe	*430*	*30.5*	*53.3*	*7.01*	*422.6*	*30.5*	*52*	*6.71*	*416.68*
080902-3-A4 - H144-4/treat/HC ZnO	*444*	*31*	*56*	*7.71*	*426*	*31*	*43.5*	*5.74*	*416*

Series G: ZIS and CdS									
	BEST DEVICES				*AVERAGE VALUES*				Av. Voc
	Voc	Jsc	FF	η	Voc	Jsc	FF	η	all cells
090502-1-B6 - H146-4/wd/ZIS/ZnSe	*363*	*30.9*	*49.7*	*5.58*	*361.1*	*30.9*	*47.4*	*5.28*	*361*
090502-2-A1 - H146-4/hw/ZIS/ZnSe	*386*	*31.6*	*54.7*	*6.67*	*355.7*	*31.6*	*49.5*	*5.57*	*355*
090502-4-A4 - H146-4/treat/CdS	*477*	*31.4*	*68.1*	*10.19*	*486.9*	*31.4*	*60.6*	*9.25*	*486*
090502-6-A4 - H146-4/evap CdS	*224*	*22.8*	*31.8*	*1.62*	*232*	*22.8*	*30.5*	*1.61*	*232*

In series A, two types of CIGS treatment are shown to improve ZIS cell efficiency. Series B confirms the major benefit of a special CIGS treatment prior to CBD CdS. In series C, some parameters are explored for CBD CdS. A 12.0% cell was obtained with the use of an i-ZnO layer; normally this layer is deleterious for non-CdS devices.

In series D, ZIS is compared to CBD CdS. As commented on previously, the special treatment for CIGS prior to CBD CdS has improved that type of device, but did not do so for ZIS. Furthermore, we have recently discovered that CIGS formed using the hybrid approach often impairs the efficiency of ZIS devices, thereby rendering such devices uncompetitive relative to devices with CBD CdS. This is currently proving to be a frustrating problem. In principle, there are aspects of the hybrid process other than sputtered Cu that could be responsible.

In series E, various buffer combinations and treatment sequences were explored. Three approaches yielded efficiencies in the 9-10% range, viz. CBD CdS, treatment of ZIS after deposition, and ZIS followed by CBD CdS. These and other results illustrate the surprising complexity of junction formation and effects of layer sequencing. One new hypothesis is that the nature of the material in contact with the ZnO is important.

The first two entries of series F report results that are reversed relative to the bulk of our findings concerning the benefit of the special treatment as applied to ZIS devices. The third entry shows a CIGS/ZnO device in which 7.7% efficiency was obtained without any buffer layer (see also [7]). Further work along these lines will be undertaken.

Series G compares ZIS (6.7%), CBD CdS (10.2%), and evaporated CdS (1.6%) buffer layers. In order to properly rank the performance of different buffer layers, we may attempt to improve the evaporated CdS process.

5.4 Effect of i-ZnO

To test whether the i-ZnO layer is really needed, we conducted an experiment to re-evaluate the merit of i-ZnO. Eight samples cut from the same CIGS run were divided into two groups with

four samples in each. One group consisted of the usual i-ZnO/n^+-ZnO layer structure as a reference, while other group consisted of the n^+-ZnO layer only (without i-ZnO). The four samples of each group received different thicknesses of CBD CdS to see if thicker CdS might eliminate the need for i-ZnO, as some researchers have claimed. Listed in Table XVII are the experimental conditions and the resulting PV parameters.

Table XVII. Comparison of cell performance with and without i-ZnO

ID	CdS Time	Voc (mV)		FF		Jsc (mA/cm2)		Efficiency	
		n-ZnO	**BothZnO**	**n-ZnO**	**BothZnO**	**n-ZnO**	**BothZnO**	**n-ZnO**	**BothZnO**
Z1539-1 & 2	15 min.	528.6	562.5	64.6	65.5	28.15	28.01	9.61%	10.32%
Z1539-3 & 4	20 min.	530.5	537.6	64.25	62.25				
Z1539-6 & 7	25 min.	527.5	557.8	63.36	63.37	28.46	28.31	9.51%	10.00%
Z1539-8 & 9	30 min.	524.7	541.9	62.27	64.62	28.43	28.22	9.29%	9.88%
Avg.		**527.8**	**550.0**	**63.62**	**63.94**	**28.35**	**28.18**	**9.47%**	**10.07%**
T-test		2 %		38 %		1 %		< 1 %	

The following conclusions can be drawn from the data shown in Table XVII (PV parameters are measured after 166 hrs. light soaking at one sun intensity):

1. Voc in the i-ZnO/n^+-ZnO layer group (our normal process) on average is about 5% higher than that in the n^+-ZnO only group (without i-ZnO). A statistical t-test shows the difference between the two groups is significant with confidence level of 98 %.

2. Difference of FF between the two groups is less than 1%. A t-test further shows the difference is not significant. However, the difference of Jsc is significant with confidence level of 99 % although the difference itself is less than 1 %. A little higher Jsc in n^+-ZnO only group is consistent with reduced optical absorption.

3. We don't see the trend, as suggested by some researchers, that the difference between these two groups is reduced by increase of CdS thickness in our experimental regime.

4. The 5% difference in efficiency between the two groups almost totally comes from the difference of Voc. The difference of efficiency is very significant (larger than 99 % confidence level) from the t-test value, as shown in Table XVII.

It should be mentioned here that all of our samples exhibit a light soaking effect. The transient behavior of PV parameters is shown later in Figs. 14a-c.

6.0 Device Properties and Performance

6.1 High efficiency devices using hybrid process in Hercules (small area) deposition system

After introducing the hybrid process in the Zeus system, we switched after a while to a similar hybrid process in the R&D Hercules system with a view to accelerating process optimization. We chose the following variables as parameters for optimization:

- x: percentage of In and Ga in the first stage evaporation (50%, 75%, 90 %)
- T: temperature of Cu selenization (400°C, 500°C, 530°C)
- t: duration of Cu selenization (10 min., 30 min., 42 min.)
- Cu ratio: adjusted via the thickness of sputtered Cu (1700A, 1900A, 2150A)
- Ga profile: adjusted by changing the starting evaporation time of Ga and In
- Ts: substrate temperature during the third stage In and Ga evaporation (500°C, 530°C).

We were encouraged that a best cell efficiency of over 13% was achieved after only a couple of months' optimization. It ties the EPV best cell record achieved with an evaporation-only process. The parameters of the three best cells are listed in Table XVIII. IV and QE curves for H139-5 B1 are shown in Figures 10 and 11.

Table XVIII. Device results obtained using hybrid process in Hercules system

ID	Voc	FF	Jsc(QE)	Efficiency
H139-5 B1	0.567 V	0.723	31.9 mA/cm^2	13.1 %
H139-3 A4	0.524 V	0.733	33.9 mA/cm^2	**13.3 %**
H139-5C1	0.553 V	0.698	31.9 mA/cm^2	12.3 %

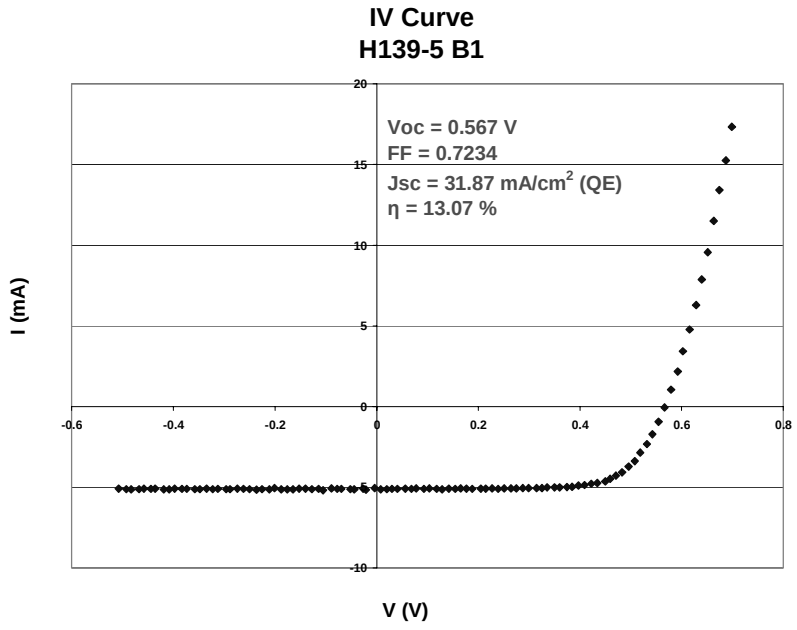

Fig. 10. I-V curve for 13.1% CIGS cell produced using hybrid process

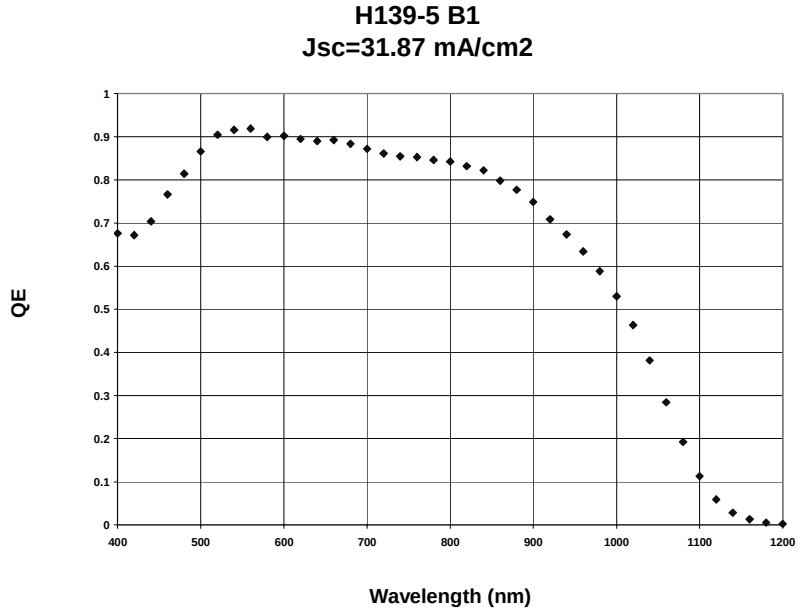

Fig. 11. Quantum efficiency for the cell of fig. 10.

A further optimization effort for the CIGS absorber layer was made with a view to improving device performance. We systematically changed the percentage of In and Ga in the first stage evaporation, with three levels (50%, 75%, 90 %) being tested. The best cells in each level are listed in Table XIX. The champion cell so far is from Level 75% (75% of In and Ga are evaporated in the 1st stage before sputtering of Cu, and 25% of In and Ga are evaporated in the final stage after Cu).

Table XIX. The best cells with different percentages of In and Ga in the first stage

Cell ID	**% In/Ga in 1st stage**	**Voc (**mV**)**	**FF**	**Jsc(**mA/cm^2**)**	**Efficiency (%)**
H146-5B A1	**75 %**	569.1	73.55	32.32	13.53
H147-5A A2	**75 %**	580.0	72.40	31.87	13.38
H139-3 A4	**75 %**	523.6	73.34	34.60	13.29
H139-5 B1	**75 %**	566.8	72.33	31.87	13.07
H146-2B2 B2	**75 %**	559.1	73.16	31.19	12.76
H146-2B1 A5	**75 %**	565.0	74.02	30.18	12.62
H147-3D D7	**75 %**	557.4	70.54	30.54	12.01
H139-4A3 B1	**75 %**	534.0	64.41	34.47	11.86
H135-5 CdS	50 %	553.9	69.69	30.15	11.64
H135-3 B5	50 %	516.1	66.41	30.96	10.61
H142-5 B1	90 %	494.2	66.43	29.95	9.83
H142-2 C5	90 %	490.6	62.32	29.11	8.90

IV and QE for H146-5B are shown in Figures 12 and 13.

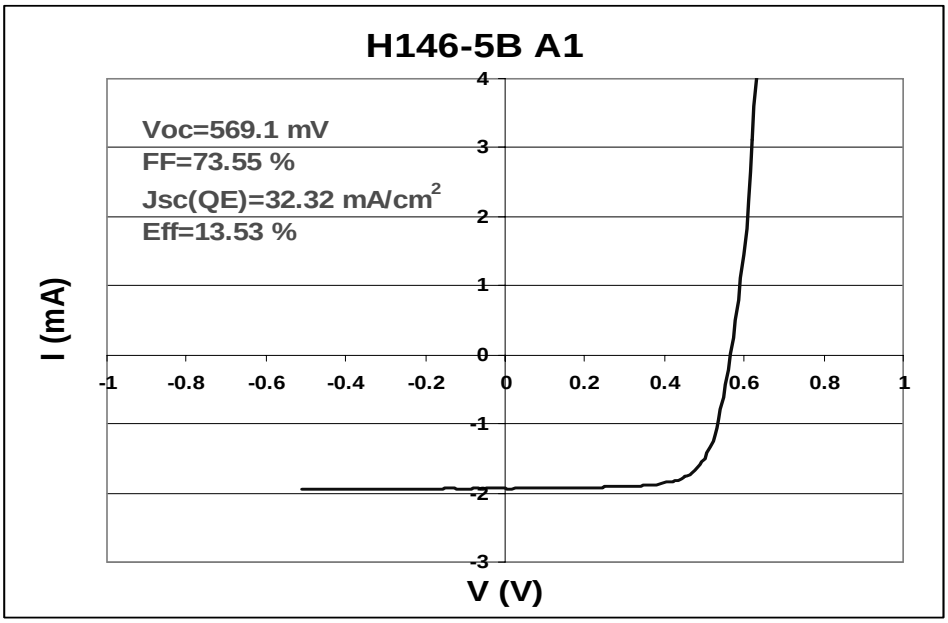

Fig. 12. I-V curve for 13.5% CIGS cell

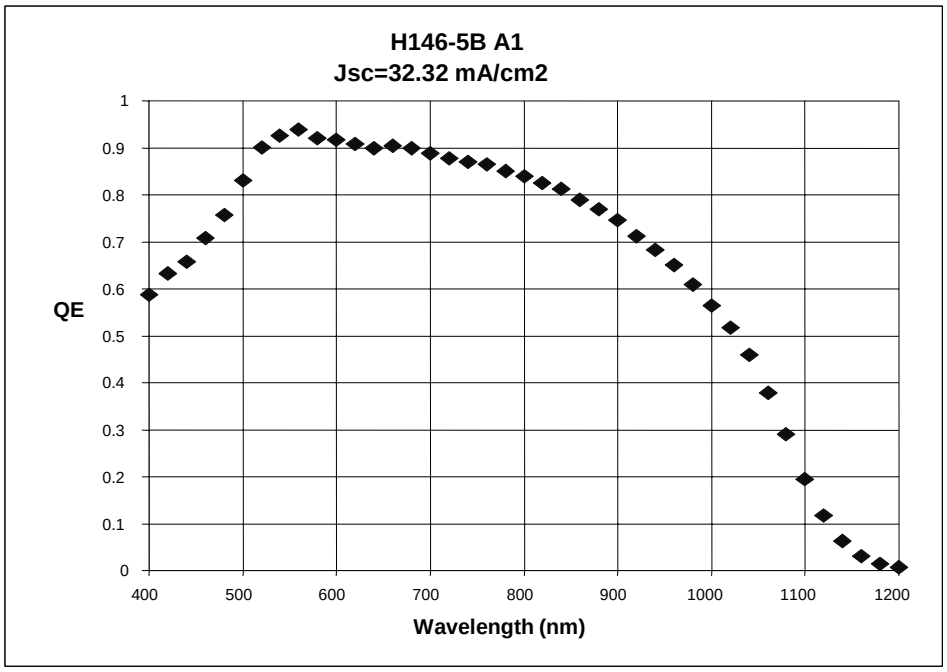

Fig. 13. Quantum efficiency for cell of fig. 12.

It is worth pointing out that all the cells made in EPV are without AR coating and without a collection grid on the ZnO (our collection distance is about double that of NREL's). We believe the efficiency for these cells in a standard device configuration with AR coating and grid would be in the range of 14%-15%.

Some Ga profiling techniques were used in making the cells listed above. We deliberately started the Ga evaporation earlier than that of the In in the 1st stage to generate a 'back-surface field' and to increase film adhesion, while we delayed Ga evaporation in the final stage to boost

Voc by increase of film bandgap in the junction region. The temperature profile during the Cu selenization step was also fine-tuned to maximize its effect.

In view of the lower V_{oc} in our cells compared to NREL's, we tested the idea of shifting more Ga from the 1st stage to the final stage to grow larger grains at the back and to further increase the bandgap near the surface. We have achieved a V_{oc} as high as over 650 mV in some devices, and we hope optimization is on the way to bring FF back to the 70% range.

In the processing of all these high performance cells, we implemented some improved non-CIGS procedures, including post-deposition treatment, improved CBD CdS, and light soaking, which are explained in Sections 4, 5.1, and 6.2.

6.2 Light soaking effects

Recently, we found that our devices now usually show significant improvement in performance after 72 hrs. light-soaking under a multi-line source at 1 sun intensity. Thus far, we have not pinned down which of the new process steps (CIGS film, post-treatment, or CdS recipe) is responsible. One set of data for comparison is listed in Table XX.

Table XX. Device performance change after light soaking

Sample ID	Parameter	Before light soaking	After light soaking	Ratio after/before
H149-2B D1	Voc	490.4	533.8	1.09
	FF	57.18	60.84	1.06
	QE	28.21	28.97	1.03
	QE-1	32.84	31.9	0.97
	Eff	**7.91**	**9.41**	**1.19**
H149-2D D3	Voc	485.5	540.2	1.11
	FF	59.56	65.21	1.09
	QE	28.12	28.06	1.00
	QE-1	32.02	30.72	0.96
	Eff	**8.13**	**9.88**	**1.22**
H149-3A A1	Voc	612.6	622.7	1.02
	FF	47.47	57.06	1.20
	QE	23.93	24.13	1.01
	QE-1	30.85	28.89	0.94
	Eff	**6.96**	**8.57**	**1.23**
H149-3B C3	Voc	588	603.3	1.03
	FF	48.07	57.26	1.19
	QE	23.76	24.41	1.03
	QE-1	29.96	29.1	0.97
	Eff	**6.72**	**8.43**	**1.26**
H149-3D A3	Voc	537.7	596.4	1.11
	FF	57.12	61.87	1.08
	QE	26.55	27.14	1.02
	QE-1	31.52	30.74	0.98
	Eff	**8.15**	**10.01**	**1.23**
H149-5A A4	Voc	560.8	578.4	1.03

	FF	59.03	65.9	1.12
	QE	25.89	26.62	1.03
	QE-1	29.43	28.68	0.97
	Eff	**8.57**	**10.15**	**1.18**
H149-5B D2	Voc	561.7	588.8	1.05
	FF	60.58	67.02	1.11
	QE	26.54	26.49	1.00
	QE-1	29.59	27.79	0.94
	Eff	**9.03**	**10.45**	**1.16**

As the data shows, the average efficiency increase is about 20 % after light soaking. Among the improvements, over 10 % is from increase of FF and a little less than 10 % is from a jump of V_{oc}, while short-circuit current density J_{sc} shows almost no change or a slight decrease in some cases. A slight optical loss was observed after light soaking from the fact that J_{sc} at reverse bias (-1V) decreases; however, the drop of J_{sc} at zero bias is partially compensated by an increase in collection efficiency. Most of the improvement persists over a few weeks, but long-term effects need to be monitored.

Plotted in Figs. 14a-c are the PV parameters as a function of light soak time for four typical samples out of eight from the groups of samples with and without i-ZnO and with different CdS thicknesses (two for each).

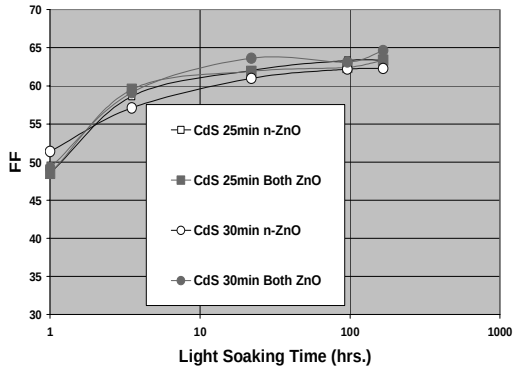

Fig. 14a. FF change with light soaking

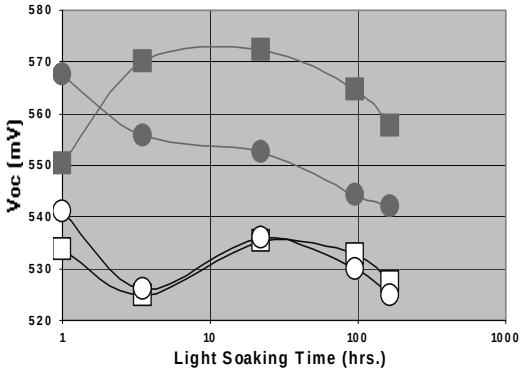

Fig. 14b. Voc change with light soaking

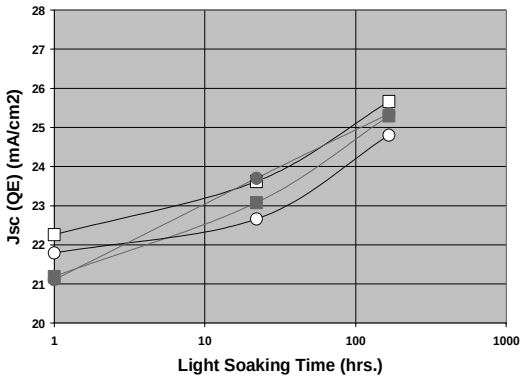

Fig. 14c. Jsc change with light soaking

The four samples exhibit similar trends, regardless of CdS thickness or the presence of i-ZnO. FF increases drastically with light soaking and keeps creeping up even after 100 hours, while V_{oc} decreases a little in most cases. It is very interesting to see short-circuit current density J_{sc} also increase significantly under light soaking. Improvement of electrical collection is believed to be the main reason for increase of J_{sc}.

7.0 Patterning and Modules

7.1 Lateral conductivity of CIGS film

One of the problems causing the most headaches in making CIGS modules (a similar problem can occur with a-Si modules) is to prevent leakage current between two segments (cells). Many module processes can cause leakage, such as Mo scribe not being clean, sharp Mo debris piled up on Mo along the scribe line, incomplete ZnO separation, scribe line overlap, and so on. Yet some modules that we made, after eliminating all of these causes mentioned above, still show a much larger leakage current than expected. Finally we realized that the CIGS material itself, deposited within the gap between two Mo segments, could short segments too. Frequently, in searching for the highest cell performance, researchers push the Cu ratio too close to unity. This might be fine at the cell level, but it can cause serious module problems if the lateral resistivity of the CIGS film is below 100 Ωcm. (CIGS sample resistivity for different groups is measured and reported in "Hall Effect and Resistivity" by University of Florida and distributed to absorber subteam).

Here is an example of the calculation of the resistance R of the CIGS film in the gap between two Mo segments:

$$R = \rho L/(td)$$

where ρ is the lateral resistivity of the CIGS film (we take it to be 50 Ωcm in this calculation), L is the Mo laser scribe line width (say 50 μm), t is the thickness of CIGS film (say 2 μm), and d is the module width (say 10 cm). A simple calculation gives R = 125 Ω. Assume the voltage between two adjacent segments is 500 mV in operation. Then, the leakage current between these

two segments due to CIGS resistance (representing a shunt path) is 500 mV/125 Ω = 4 mA. The operating current in such a module is about 142.5 mA (= 30 mA/cm2*10 cm* 0.475 cm Mo width). Thus the leakage current is about 3% of the operating current, and represents a noticeable shunt. (This result is independent of module width.) This example suggests that we should keep the Cu ratio well below unity to keep CIGS lateral resistivity above 100 Ωcm.

This leakage current could be even larger if the Cu layer in the CIGS in the gap between Mo segments is not sufficiently diffused and reacted with In, Ga and Se. Several directions to eliminate or reduce the CIGS shunting path are listed here:

- Increase the first IGS thickness by increasing total film thickness and/or increase its percentage x of total thickness.
- Reduce Mo thickness.
- Optimize the temperature and time for Cu selenization before depositing the second part of the IGS.

7.2 Issue of i-ZnO for production

In our normal module processing described in Section 7.6, deposition of i-ZnO by sputtering (step 9) is the least time-effective one. It only takes two minutes to sputter deposit a couple of hundred Angstrom thick i-ZnO film, however, it costs a couple of hours overhead to pump down the sputtering system. Unlike the case of device processing, where no vacuum break is required between the i-ZnO and n-ZnO, in module processing we have to break vacuum between the i-ZnO and n-ZnO because the CIGS scribing (step 10) must be performed *after* the i-ZnO layer and before the n-ZnO layer.

Rather than eliminating it, we hope to find a non-vacuum process to replace the sputtered i-ZnO, since devices with two ZnO layers consistently perform better than those without the i-ZnO layer. One thought is to replace i-ZnO with the high bandgap material ZnS, which could be processed either by CBD or by spray. In our first test, we applied a sprayed ZnS layer right after CBD CdS, and then sputtered an n-ZnO film to finish the window layers. However, the performance of our first try was disappointing. Both V_{oc} and FF in the test exhibited lower values than those in n-ZnO only and two-ZnO layers structures. More experiments are planned.

7.3 Laser scribing

With a view to reducing the dead area, and to making a more conductive interconnect contact, laser scribing was evaluated once again. A Spectra-Physics X30S-532Q laser with wavelength 532 nm is used to scribe both CIGS and ZnO.

We set the goals for CIGS scribing to be:

1. The laser scribe width should be less than 100 μm.
2. The laser should strip off all the CIGS so that the Mo layer is exposed.
3. The laser should not totally strip off the Mo layer.
4. The Mo -n-ZnO interconnection should have low contact resistance.

So far we have been able to access the whole scribe spectrum from a very shallow cutting of the CIGS to stripping off all of the Mo layer by process optimization, including laser power, laser repetition rate, laser focus and speed of X-Y table. The scribe width is in the desired range. However, we have not been able to integrate the CIGS laser scribe with submodule processing due to lack of an alignment fixture. A test structure was designed recently for speeding up process optimization, and its usefulness will be tested soon.

Our goals for the ZnO laser scribe are:

1. Total separation of ZnO
2. No deterioration of device performance.

Many small isolated devices were used to test ZnO scribing conditions. We changed laser process parameters starting with very shallow cutting, and searched for conditions in which resistance R between two separated areas defined by the ZnO scribe line is larger than 10 kΩ. Next, we compared device performance change before and after scribe by paying special attention to change of shunting resistance, V_{oc}, and FF. Some test conditions and results are listed in Table XXI.

Table XXI. Test of ZnO laser scribe

Test	Voc-A	Voc-B	FF-A	FF-B	Rsc-A	Rsc-B	Voc	FF	Rsc
1	353.3	357.5	36.47	37.3	3.55	4.37	-1.2%	-2.3%	-23.1%
1	353.1	359.2	36.09	37.8	3.38	4.05	-1.7%	-4.6%	-19.8%
2	361.1	358.3	35.52	37.8	4.08	4.51	0.8%	-6.4%	-10.5%
2	364.4	364	37.49	39.3	3.99	4.66	0.1%	-4.8%	-16.8%
3	364	358.9	41.25	43	5.61	7.69	1.4%	-4.2%	-37.1%
3	301.2	296.2	33.69	34	2.47	2.73	1.7%	-0.9%	-10.5%
4	362.4	351.6	41.69	45.2	5.45	6.81	3.0%	-8.3%	25.0%-
4	400.7	396.3	34.52	37.3	3.1	3.76	1.1%	-8.1%	-21.3%
5	361.3	353.8	40.57	43.4	4.85	6.69	2.1%	-6.9%	-37.9%
5	371.5	386	40.03	32.4	4.55	2.5	-3.9%	19.1%	45.1%
6	364.8	378	36.75	35.9	3.32	3.86	-3.6%	2.2%	-16.3%
6	371.4	369.8	36.96	37.7	3.77	3.96	0.4%	-1.9%	-5.0%
7	334.8	328.9	44.82	45.5	6.02	7.07	1.8%	-1.6%	-17.4%
7	348.4	352.1	42.58	42.9	6.92	7.69	-1.1%	-0.7%	-11.1%
8	349.2	350.6	43.36	45	5.69	6.03	-0.4%	-3.7%	-6.0%
8	363.7	362.8	36.97	37.6	4.07	4.32	0.2%	-1.7%	-6.1%
9	352.5	352.4	41.49	42.3	5.87	6.12	0.0%	-2.0%	-4.3%
9	371	368.4	36.62	37	4.14	3.96	0.7%	-0.9%	4.3%
10	362.6	418.5	28.95	27.3	1.81	1.88	-15.4%	5.6%	-3.9%
10	390.6	404.3	30.17	30.1	2.29	2.12	-3.5%	0.1%	7.4%

The results clearly show that with test conditions 8, 9, and 10, device performance deteriorates less severely than with other conditions, which give us a starting point for the next round of optimization.

7.4 Alternative interconnect methods

In the standard CIGS module process, a scribe line to remove the CIGS film, either by mechanical or by laser means, is needed prior to deposition of the conductive window film (ZnO) to serve as an interconnection path between adjacent cells. However, mechanical scribing risks scratching the substrate glass, increasing the risk of breakage during module lamination, while laser scribing might generate rough edges, and these can cause shunting paths. An alternative way to make the interconnection is being explored.

7.5 Segment width calculations

By taking into account the two major module losses, I^2R loss due to resistance of CTO and interconnection, and current loss due to dead area, we developed a model for optimization of cell width. A graph for effective power, which is defined as the ratio of the module output power with these two major losses to the output power without these losses, versus cell width is plotted in Fig. 15. Because we had a relatively wide dead area of about 0.8 mm width caused by our manual mechanical scribing for CIGS and ZnO, a total cell width of 6.6 mm was chosen for the immediate mini-module process. With ZnO sheet resistance about 10 Ω/square, the effective power for such a cell width is seen from Fig. 15 to be about 1-2% lower than that for an optimized width of 5.3 mm, but the fewer lines makes the manual operation easier.

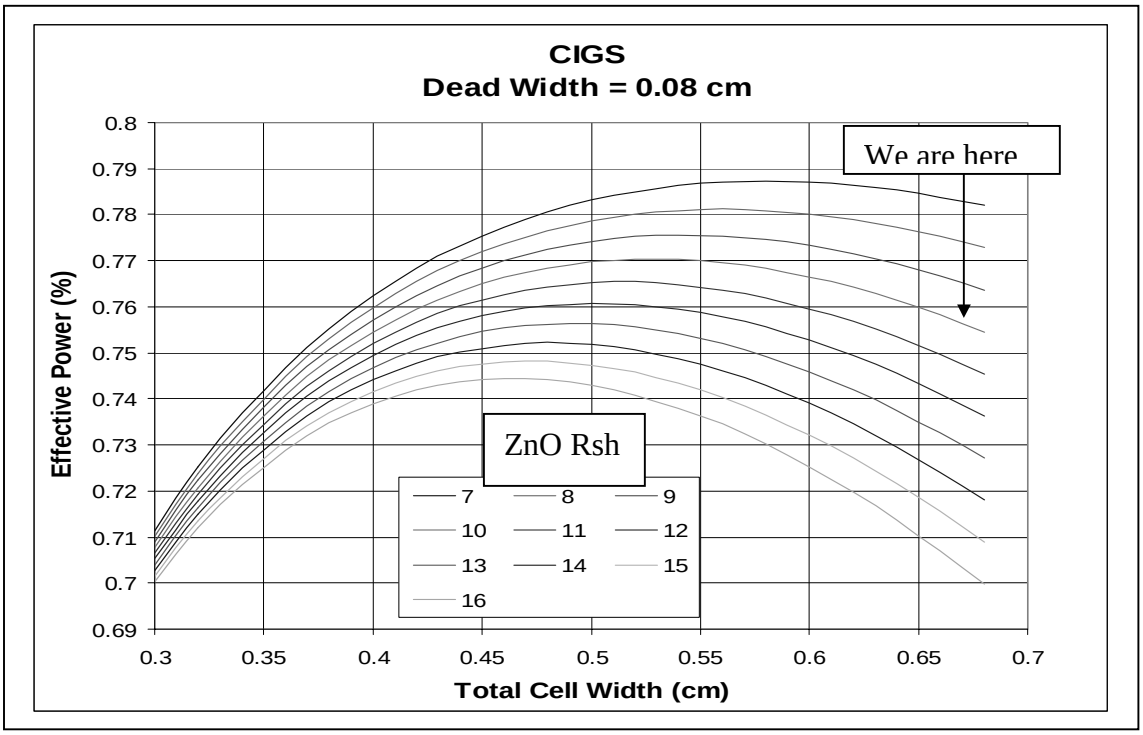

Figure 15. Optimization of segment width

7.6 Submodule process and fabrication of mini-modules using hybrid CIGS process

Our current submodule process consists of the following steps:

1. Prepare glass (cut, seam, wash, and store)

2. Sputter Cr and Mo
3. Laser Mo and check isolation
4. First In, Ga, and Se
5. Sputter Cu
6. Selenize Cu, and second In, Ga, Se
7. Post-CIGS treatment
8. CBD CdS
9. Sputter i-ZnO
10. Mechanical scribing of CIGS
11. Sputter n^+-ZnO
12. Mechanical scribe of ZnO/CIGS and check
13. Light soak
14. Measure I-V
15. Diagnostics

We restarted our module process again after a reasonably good hybrid CIGS recipe was established in the R & D Hercules system. Because of the relatively short distance of 18 inches between substrate and indium (gallium) sources in the Hercules system, less than perfect CIGS uniformity is observed for large substrates. Therefore, we decided to start by fabricating mini-modules with a dimension of 2" x 4".

So far, the efficiency of our best submodule (H156-2) is 9 % (active area efficiency 10.2 %). The submodule has 13 cells and an aperture area of 38.7 cm^2. Its IV curve is plotted in Fig. 16.

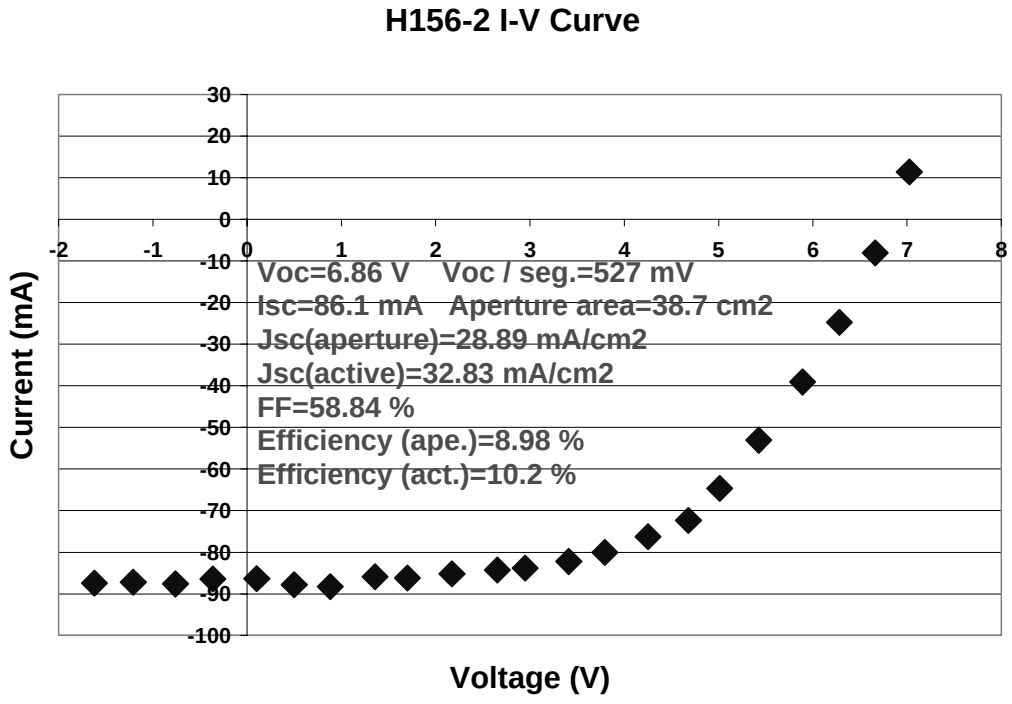

Fig. 16. I-V curve for 9.0% submodule H156-2 (13 segments, 38.7 cm^2 aperture area)

Listed for comparison in Table XXII are PV parameters from our recent best performance cell and submodule.

Table XXII. Comparison of device and submodule performance

	ID	V_{oc}/cell (mV)	FF (%)	J_{sc} (mA/cm^2)	Efficiency (%)
Best device	H146-5	569.1	73.55	32.32	13.5
Best submodule	H156-2	527.0	58.84	28.89	9.0
Difference %		-7.4 %	-20 %	-11 %	-36.3 %

A low dark leakage current of about 0.01 mA at -5V in submodule H156-2 was obtained, which is only 0.01 % of I_m (the current at the maximum power point). Therefore, we don't expect that module shunt resistance causes any V_{oc} drop. So the 7.4 % drop in V_{oc} shown in Table XXII probably stems from the different CIGS run rather than the module process. Cell width modeling (Fig. 15) suggests that the effective power loss should be about 24% from the device level in our case. Contributing to this, J_{sc} will drop 12% due to dead area, which is very close to the 11 % figure shown in Table XXII, while FF should lose 12 % due to series resistance, which is significantly less than the observed figure of 20% shown in Table XXII. This indicates that CIGS quality or uniformity for run H156, larger interconnect resistance, or unexpectedly higher ZnO sheet resistance must be examined for their possible roles in our submodule performance. Previously reported diagnostic techniques will be employed in these analyses [8].

In another submodule processed lately, H157-4, an average V_{oc} of 571 mV per cell was achieved, even though a large leakage current in three out of thirteen cells was found. For comparison, V_{oc} measured from devices cut from this submodule was 591 mV.

8.0 Phase I Summary

EPV, Inc.
Thin-Film CIGS Photovoltaic Technology
Subcontract No. ZDJ-2-30630-21

- A hybrid CIGS process (involving Cu deposition by sputtering) was explored, with the goal of improving uniformity of CIGS thickness and composition. The remaining elements, In, Ga, and Se, continue to be delivered by evaporation, and in the case of large area coating, using linear sources.

- An improved thickness distribution on large area plates was realized for CIGS produced by the hybrid process.

- Theoretical modeling of vapor distribution by manifolds was conducted, as a contribution to studying linear source deposition uniformity.

- A method for quantifying the concentration of Zn as an impurity in CIGS was developed using ICP OES.

- An extensive survey of post-deposition treatments of CIGS was made. A very useful, although wet, treatment was identified that seems always to improve the performance of devices processed using CBD CdS.

- Optimization of EPV's procedure for CBD CdS was conducted. Improved device performance was realized after a change from Cd acetate to Cd sulfate, and an increase in the S/Cd ratio.

- Using the hybrid CIGS process, post-deposition treatment, and the improved CBD CdS recipe, cells up to 13.5% efficiency (569 mV, 32.3 mA/cm^2, FF 73.5%) were produced (no AR coating). These devices were found to improve upon light soaking.

- Using EPV CIGS prepared by evaporation of all elements, a 10.1% cell was produced using an evaporated zinc indium selenide (ZIS) buffer layer, and 8.6% using evaporated In_2S_3.

- It was found that CIGS produced by the hybrid process often does not respond well to the ZIS buffer layer.

- Spray deposition was used to prepare good-looking films of CdS, ZnS, and In_2S_3. Devices using spray CdS reached 5.6% efficiency.

- Some promising results were obtained from a renewed study of laser scribing of CIGS and ZnO.

- A mini-module with laser-scribed Mo, but mechanically-scribed CIGS and ZnO, was produced having an aperture area efficiency of 9.0%.

CIGS DEVICES WITH ZIS, In_2S_3, AND CdS BUFFER LAYERS

A.E. Delahoy[1], M. Akhtar[1], J. Cambridge[1], L. Chen[1], R. Govindarajan[1], S. Guo[1], and M.J. Romero[2]
[1]Energy Photovoltaics, Inc.
P.O. Box 7456, Princeton, NJ 08543, USA
Tel. 609-587-3000; fax 609-587-5355; e-mail: a.delahoy@epv.net
[2]National Renewable Energy Laboratory, Golden, CO 80401, USA

ABSTRACT

The device performances of Cu(In,Ga)Se_2 solar cells are compared as a function of various buffer layers applied by thermal evaporation that are considered as candidates to replace the conventional CdS buffer layer applied by chemical bath deposition. The buffer layers include $ZnIn_2Se_4$ (ZIS), In_2S_3, and ZnSe. Devices with CdS and ZIS buffers are also studied by EBIC and cathodoluminescence.

INTRODUCTION

The highest efficiency CIGS solar cells possess the structure glass/Mo/CIGS/CdS/i-ZnO/n-ZnO:Al and are conventionally fabricated using a CdS buffer layer prepared by chemical bath deposition. The latter process is not manufacturing-friendly because of the liquid waste and the use of cadmium. These two issues represent significant hindrances for CIGS PV manufacturing. As part of an on-going effort to solve these problems, EPV is investigating alternative buffer layers prepared by vacuum evaporation. We have previously reported the use of $ZnIn_xSe_y$ (ZIS) as a buffer material [1]. This material was selected for investigation since In and Se are already present in CIGS, Zn is an n-type dopant, and promising efficiencies had been reported using $ZnIn_2Se_4$ as a buffer layer [2]. This earlier work employed three-source co-evaporation of Zn, In, and Se. Our approach has been to synthesize $ZnIn_2Se_4$ as a bulk material and use it as a single evaporation source [1]. Advantages of this method include simplification of the deposition hardware and of process control. In this paper, we compare the performance of CdS, ZIS, and In_2S_3 as buffer materials. In addition, we briefly explore ZnSe and CdSe.

EVAPORATION OF ZIS

The evaporation behavior of $ZnIn_2Se_4$ was investigated by monitoring the film deposition rate as a function of source temperature during the complete evaporation of a fresh charge of $ZnIn_2Se_4$. A small emission peak was observed at a source temperature of about 290°C, followed by the principal emission peak at about 850-860°C, with no other peaks at higher temperatures (see Fig. 1). EDS analysis of material captured during the initial emission revealed it to be selenium. We do not yet know for certain whether this initial Se is helpful, harmful, or neutral with regard to cell performance.

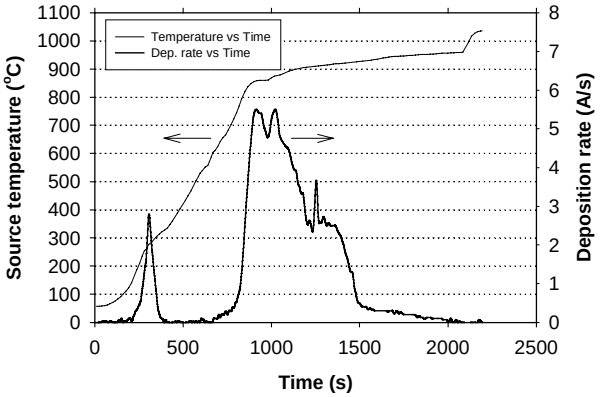

Fig. 1. ZIS deposition rate as a function of evaporation time and source temperature.

DEVICE PERFORMANCE

Using samples of CIGS/Mo/glass cut from pieces deposited in EPV CIGS run H106, we prepared reference devices using CBD CdS, and companion devices with ZIS and In_2S_3 buffer layers. In these runs the buffer material was evaporated from a graphite crucible, the form of the material being granules for ZIS and powder for In_2S_3. Devices were completed by sputtering of a transparent conducting oxide consisting of ZnO:Al. Our previous work indicated that the optimum substrate temperature for ZIS deposition was in the neighborhood of 200°C, and a series of four ZIS runs of identical thickness were made to try to pin down more precisely the optimum temperature. The ZnO was sputtered onto these four substrates simultaneously. The results of this study are summarized in Table 1.

Table 1. Dependence of ZIS/CIGS cell parameters on substrate temperature for ZIS deposition

T_s (°C)	Av. V_{oc} (mV)	Av. FF (%)	J_{sc} from QE (mA/cm^2)	Av. eff. (%)	Best eff. (%)
175	486.2	63.5	28.9	8.88	9.1
185	490.5	63.9	29.0	8.89	9.2
197	491.9	65.0	29.7	9.42	10.1
210	493.9	64.3	28.4	9.05	9.4

A best cell efficiency of 10.1% was achieved at a ZIS deposition temperature of 197°C, and high cell yields were obtained in all four experiments.

For In_2S_3 buffers, two temperatures (185°C and 200°C) and two thicknesses were explored, with the best cell efficiencies for each condition ranging from 7.3% to 8.6%. The best cell results for all three types of buffer layer are summarized in Table 2.

Table 2. Best cell results with CdS, ZIS, and In_2S_3 buffer layers deposited on CIGS from run H106.

Buffer	Deposition (T_s °C)	V_{oc} (mV)	J_{sc} from QE mA/cm	FF (%)	Eff. (%)	Eff rel. to CdS
CdS	CBD 77°	536	33.5	67.1	12.0	100
ZIS	Evap 197°	503	29.7	67.4	10.1	84
In_2S_3	Evap 185°	497	26.8	64.5	8.6	72

Figure 2 shows the I-V curves for these cells, and Figure 3 their QE spectra. It may be noted that in this series of experiments the efficiencies of ZIS and In_2S_3 reached 84% and 72% of the efficiency obtained with CBD CdS.

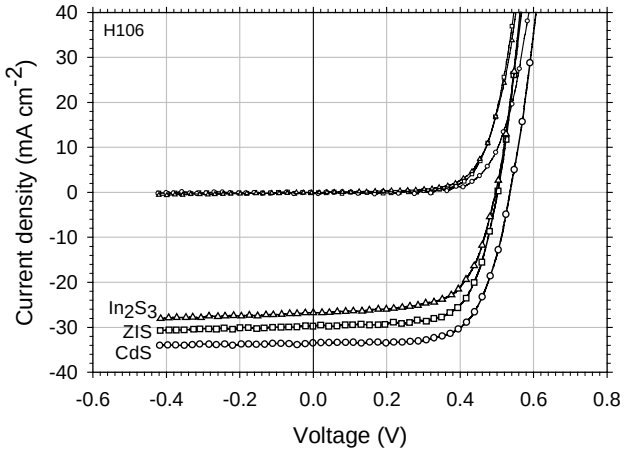

Fig. 2. I-V curves for the best cells with CdS, ZIS, and In_2S_3 buffer layers

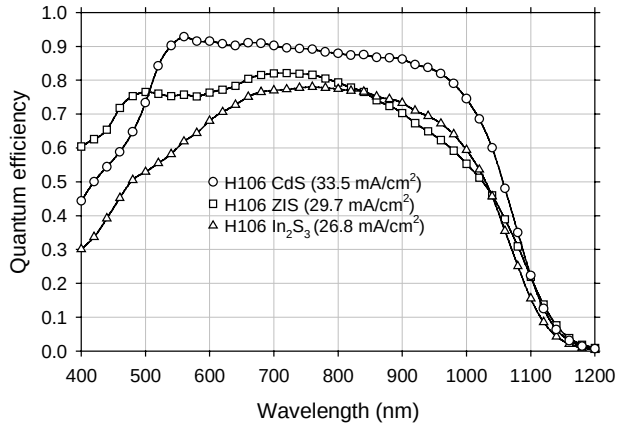

Fig. 3. Quantum efficiency curves for the above cells.

As can be seen from Fig. 3, good short wavelength response can be obtained with a ZIS buffer as quite thin ZIS layers are sufficient to obtain their function. Nevertheless, the peak QEs obtained with the evaporated buffer layer process represented in figure 3 are lower than that obtained with CdS.

Subsequent to these experiments, a modified deposition procedure was discovered that appeared to eliminate the reduction of peak QE. Table 3 shows the performance of cells utilizing this modified procedure. (Unfortunately, the CIGS employed in these studies was prepared differently and was of inferior quality relative to the previous study.) Also, a wider variety of materials was surveyed, including ZIS, ZnSe [4], and CdSe. Our experience has been that, although it serves as a functional buffer material, ZnSe generally yields devices somewhat inferior to those using ZIS (see Table 3).

Table 3. Performance of various buffers deposited with modified recipes on CIGS from runs H133 and H128.

Buffer	Deposition (T_s °C)	V_{oc} (mV)	J_{sc} from QE mA/cm^2	FF (%)	Eff. best (%)	Eff rel. to CdS
CdS[1]	CBD 77°	547	32.0	59.3	10.4	100
ZIS[1]	Evap 197°	508	30.4	62.8	9.7	93
CdSe[1]	Evap 197°	467	22.2	50.9	5.3	51
ZIS[2]	Evap 197°	464	31.7	67.4	9.9	-
ZnSe[2]	Evap 197°	465	29.5	65.9	9.0	-

[1]CIGS from run H133; [2]CIGS from run H128

It is noteworthy that, using the modified procedure, the performance of ZIS relative to CBD CdS has now reached 93% (9.7% efficiency versus 10.4%). We find that while the V_{oc} obtained with ZIS is often 6-7% lower than that obtained with CBD CdS, the ZIS cells frequently exhibit a somewhat higher fill factor. Another shortfall of ZIS that is often, but not always, observed, is a more pronounced long-wavelength fall off. This is evident, for example, in the QE curves in figures 3 and 4. This observation suggests that the chemical bath treatment often results in a longer minority carrier diffusion length.

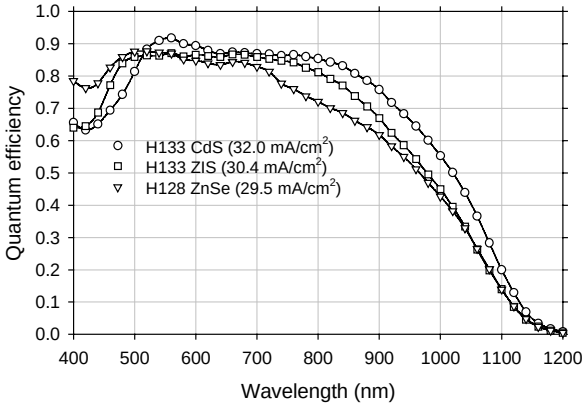

Fig. 4. Quantum efficiency curves for three cells from Table 3.

EBIC AND CL

We have further investigated ZnO/ZnInSe/Cu(In,Ga)Se_2 solar cells produced at EPV using high-resolution electron-beam-induced current (EBIC) and cathodo-luminescence (CL). These cells were compared to CIGS solar cells with CdS buffer layers produced at NREL. EBIC measurements were carried out in a field-emission scanning electron microscope (FESEM JEOL 6320F) at 1 keV of electron-beam energy. Cross-sectional EBIC observations performed at such low electron-beam energy provided lateral resolutions of 50 nm. The CL measurements were performed in a conventional SEM (JEOL 5800) equipped with an OXFORD system2. A schematic of the measurements is shown in Figure 5.

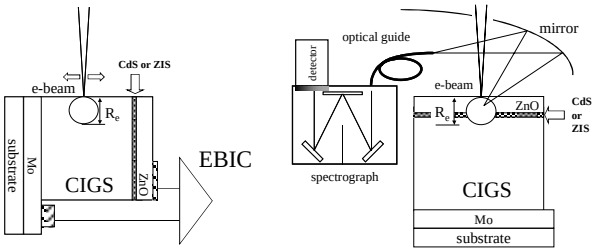

Fig. 5. Schematic of the EBIC and cathodoluminescence measurements.

Energy transferred from the highly energetic primary electrons results in the generation of a highly localized source of carriers, with a range of penetration R_e. The excess carriers diffuse, and those carriers that are collected under the field provided by the CIGS/CdS or CIGS/ZIS heterojunction yield a current that is subsequently amplified. Those that recombine radiatively lead to the cathodoluminescence.

Figure 6 shows in detail the ZnO/CdS/CIGS/Mo structure. The measured induced current shown in Fig. 6 is representative of high-efficiency, CIGS solar cells produced at NREL. EBIC imaging at high resolution confirms that the CIGS/CdS interface behaves as an ideal heterojunction. The maximum of induced current is accordingly well defined at the interface.

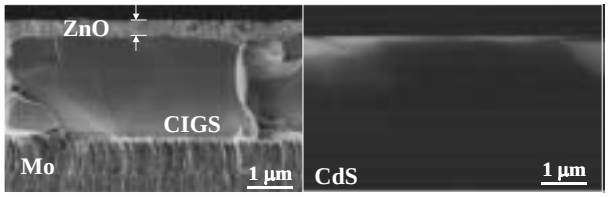

Fig. 6. Secondary-electron and EBIC images from the ZnO/CdS/CIGS solar cell. E_b = 1 keV and (electron-beam current) I_b = 100 pA.

Figure 7 shows the secondary-electron and EBIC images for the cell with ZIS as buffer layer. EBIC observations suggest that there is a non-ideal junction at the ZIS/CIGS because the depletion region is extended deeper in the film.

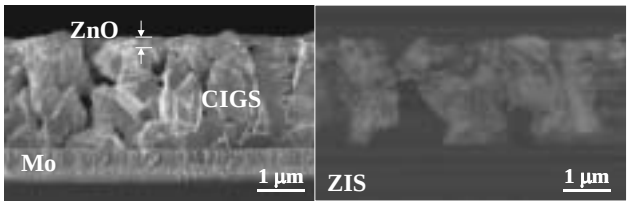

Fig. 7. Secondary-electron and EBIC images from the ZnO/ZIS/CIGS solar cell. E_b = 1 keV and I_b = 100 pA.

Figure 8 shows the EBIC as a function of the distance to the CdS or ZIS buffer layers. Because of the extremely low electron-beam energies used here, the distribution of the induced current nearly corresponds to the distribution of the charge-collection efficiency, ϕ. For the EPV device, we found that the maximum of ϕ is located deep within the absorber, approximately 1500 nm from the ZIS/CIGS interface. In addition, the pronounced decay of the current closer to the interface suggests a high surface recombination velocity, estimated at 10^5 - 10^6 cm s^{-1}.

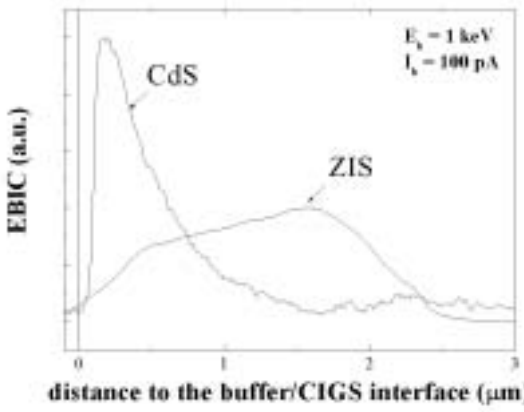

Fig. 8. Averaged EBIC as a function of the distance to the buffer/CIGS interface.

CL spectroscopy was employed for investigating the effects of buffer layer deposition on electronic states at both the CdS/CIGS and ZIS/CIGS interfaces. At 5 keV of beam energy, the excitation is almost confined to these interfaces.

Figure 9 shows the evolution of the spectra from the surface of the CIGS films under development of the CdS buffer layer, which is represented by the deposition time. The broad emission at the early stage of deposition (t = 3 min) might be associated with donor-to-acceptor (DAP) transitions from $V_{Cu\text{-}Se}$ divacancies to V_{Cu}, as the surface of the absorber is copper depleted. If Cd is incorporated into the V_{Cu}, we should observe a shift to higher photon energies by the consumption of copper vacancies, as observed. The shoulder at lower photon energies seen when the CdS completely covers the surface of the absorber might be related to a recombination inherent to energy levels related to Cd impurities. Whether Cd is incorporated into CIGS or not should be corroborated by other techniques, but CL spectroscopy shows that CdS deposition definitely modifies the electronic states at the surface of the absorber.

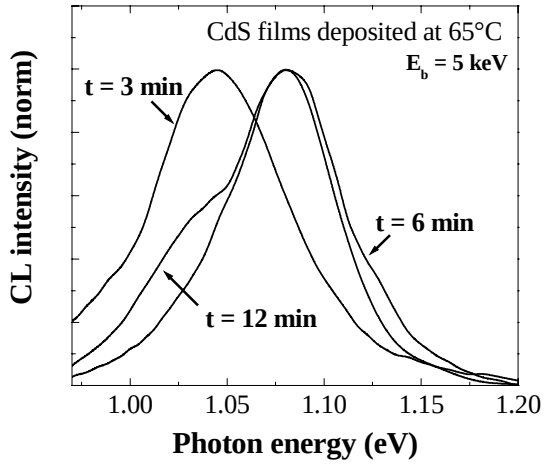

Fig. 9. Evolution of the CL spectra from the surface of the CIGS films under development of the CdS buffer layer (represented by the deposition time).

Figure 10 shows the spectra recorded from the ZIS/CIGS devices. The spectra from the bulk of the film were excited with electron-beam energies above 20 keV. The shift to higher photon energies observed when increasing the electron-beam current suggests a DAP transition as observed for CdS/CIGS cells. The spectra closer to the ZIS/CIGS interface are similar to those from the bulk at high excitation, although the emission is wider, suggesting a higher concentration of nonradiative recombination centers near the interface. ZIS deposition does not produce novel radiative transitions.

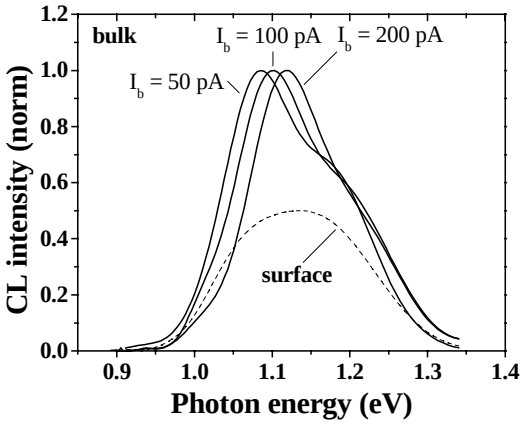

Fig. 10. CL spectra recorded from the bulk and the surface of the ZIS/CIGS device.

DISCUSSION

The difficulty of replacing CBD CdS is that it is not just a layer, but that the layer and process together confer many separate and distinct benefits. These are thought to include:

a) cleaning of the CIGS surface;
b) conformal coverage;
c) protection against sputter damage;
d) in-diffusion of Cd (possibly by Cu-Cd ion exchange);
e) CIGS defect passivation (surface & grain boundaries);
f) provision of a high resistivity buffer layer to improve V_{oc};
g) provision of a conduction band edge 0.2-0.3eV higher than that of CIGS to avoid recombination under forward bias [5], and an appropriate conduction band edge step at the ZnO interface.

The modified processing described in the device performance section was designed to address some of these issues. If all of the above benefits can be duplicated using dry processing, then we are confident that ZIS can be engineered to match the efficiency of CBD CdS.

Another important concern is stability. We have quite clearly observed that some devices using ZIS buffers are stable over time, while others degrade. At present, we believe this is largely a function of the CIGS. Also remaining to be done is SIMS profiling to examine the distribution of Zn and Cu in the CIGS after ZIS deposition.

CONCLUSIONS

$ZnIn_2Se_4$ was found to sublime at a source temperature of 850°C. Using a previous deposition recipe for ZIS, CIGS solar cells were fabricated having an efficiency of 10.1%. Relative to the efficiency of cells with CBD CdS, ZIS and In_2S_3 buffers achieved performance levels of 84% and 72%, respectively. A modified process for ZIS allowed us to increase its relative performance to 93% of CBD CdS. High-resolution EBIC studies of a ZIS device suggested that peak collection occurred for generation 1.5μm deep into the CIGS, while CL spectroscopy was consistent with a high surface recombination velocity. CL also showed that CdS deposition definitely modifies the electronic states at the surface of the absorber.

ACKNOWLEDGMENTS

This work was supported in part by the U.S. DOE under subcontract no. ZAK-8-17619-21 with NREL.

REFERENCES

[1] A. Delahoy, M. Akhtar, J. Bruns, A. Ruppert, L. Chen, Z. Kiss "Ternary Source Materials for CIGS Buffer Layers," *Proc. 16th European PVSEC*, 2000, pp. 767-770.
[2] M. Konagai, Y. Ohtake, and T. Okamoto, *MRS Symp. Proc. Vol.* ***426*** (1996) 153-163.
[3] M.J. Romero, M.M. Al-Jassim, R.G. Dhere, F.S. Hasoon, M.A. Contreras, T.A. Gessert and H.R. Moutinho, *Prog. Photovolt: Res. Appl.* 2002, **10**, pp. 1-11.
[4] F. Engelhardt, L. Bornemann, M. Kontges, Th. Meyer, J. Parisi, E. Pschorr-Schoberer, B. Hahn, W. Gebhardt, W. Riedl, F. Karg and U. Rau, *2nd World Conf. PVSEC*, 1998, pp. 1153-1156.
[5] T. Minemoto, H. Takakura, Y. Hamakawa, Y. Hashimoto, S. Nishiwaki and T. Negami, *Proc. 16th European PVSEC*, 2000, pp. 686-689.

ACKNOWLEDGMENTS

EPV wishes to thank the following members of EPV's technical staff and support team who contributed to this work: M. Akhtar, J. Cambridge, L. Chen (Senior Scientist), D. Chorobski, A. Delahoy (Principal Investigator), A. Foustotchenko, R. Govindarajan, S. Guo, Z. Kiss, R. Lyndall, R. Saramak, F. Sheppard, and F. Ziobro.

The following individuals (and institutions) are also acknowledged for their analyses, experiments, advice, or interest: S. Asher, M. Contreras, K. Ramanathan, R. Noufi, H. Ullal, K. Zweibel (National Renewable Energy Laboratory), J. Sites (Colorado State University), A. Rockett (University of Illinois), R. Birkmire, W. Shafarman (Institute of Energy Conversion/University of Delaware), L. Olsen (Washington State University), T. Anderson, S. Li (University of Florida).

Thanks are due also to all members of the National CIS Team for their collaborations and discussions.

Finally, EPV thanks the US DOE for support under subcontract ZDJ-2-30630-21with NREL.

PUBLICATIONS CITED IN THIS REPORT RESULTING FROM THE EPV THIN FILM PARTNERSHIP WORK IN CIGS

[1] A.E. Delahoy, J. Cambridge, L. Chen, and Z. Kiss "Thin Film CIGS Photovoltaic Technology," Final Technical Report, NREL/SR-520-31739 (2002).
[2] A.E. Delahoy, J.S. Britt, A.M. Gabor, and Z.J. Kiss, *AIP Conf. Proc. Vol.* ***353*** (AIP, NY, 1996) pp. 3-11.
[3] A. Delahoy, J. Bruns, L. Chen, M. Akhtar, Z. Kiss "Advances in Large Area CIGS Technology," *Proc. 28th IEEE PV Specialists Conference*, September 15-22, 2000, Anchorage, AK, pp. 1437-1440.
[4] Delahoy, A.E., Akhtar, M., Cambridge, J., Chen, L., Chorobski, D., Govindarajan, R., Guo, S., Kiss, Z., Ruppert, A., Anna Selvan, J.A., Ziobro, F., "Aspects of Large Area CIGS Technology," *Proc. NCPV Program Review Meeting*, Lakewood, CO, October 14-17, 2001 (NREL/EL-520-31065).
[5] A. Delahoy, M. Akhtar, J. Bruns, A. Ruppert, L. Chen, Z. Kiss. "Ternary Source Materials for CIGS Buffer Layers," *Proc. 16th European PVSEC*, 1-5 May 2000, Glasgow, UK, pp. 767-770.
[6] A.E. Delahoy, M. Akhtar, J. Cambridge, L. Chen, R. Govindarajan, S. Guo, and M.J. Romero "CIGS Devices with ZIS, In_2S_3, and CdS Buffer Layers" *Proc. 29th IEEE PV Specialists Conference*, May 20-24, 2002, New Orleans, LA, pp. 640-643.
[7] A.E. Delahoy, A.F. Ruppert, and M. Contreras, *Thin Solid Films* **361-362** (2000) 140-144.
[8] A.E. Delahoy, D. Chorobski, F. Ziobro, Z.J. Kiss, *AIP Conf. Proc. Vol.* ***462*** (AIP, NY, 1999) 144-151.

OTHER REFERENCES

[R1] A.E. Delahoy and Z.J. Kiss "Photovoltaics – heading towards thin films" Photovoltaics Bulletin (Elsevier Advanced Technology, Oxford, ISSN 1473-8325) Nov. 2001, pp. 8-12.
[R2] James Groelinger and Alan Delahoy "The Future of Thin Film PV" SolarAccess.com RE Outlook 2003 (Jan. 17, 2003) http://www.solaraccess.com/news/story?storyid=3448
[R3] M.A. Contreras, B. Egas, K. Ramanathan, J. Hiltner, A. Swartzlander, F. Hassoon, and R. Noufi, *Prog. Photovolt: Res. Appl.* **7**, 311-316 (1999).
[R4] I.L. Eisgruber et al., *Conf. Proc. 28th IEEE PVSC*, (2000) pp. 684-687.
[R5] R.D. Wieting, *Conf. Proc. 29th IEEE PVSC*, (2002) pp. 478-483.

REPORT DOCUMENTATION PAGE

Form Approved
OMB NO. 0704-0188

1. AGENCY USE ONLY (Leave blank)	2. REPORT DATE	3. REPORT TYPE AND DATES COVERED
	May 2003	Annual Technical Report 15 November 2001–14 November 2002

4. TITLE AND SUBTITLE
Advanced CIGS Photovoltaic Technology: Annual Technical Report, 15 November 2001–14 November 2002

5. FUNDING NUMBERS
PVP35001
ZDJ-2-30630-21

6. AUTHOR(S)
A.E. Delahoy and L. Chen

7. PERFORMING ORGANIZATION NAME(S) AND ADDRESS(ES)
Energy Photovoltaics, Inc.
P.O. Box 7456
Princeton, NJ 08543

8. PERFORMING ORGANIZATION REPORT NUMBER

9. SPONSORING/MONITORING AGENCY NAME(S) AND ADDRESS(ES)
National Renewable Energy Laboratory
1617 Cole Blvd.
Golden, CO 80401-3393

10. SPONSORING/MONITORING AGENCY REPORT NUMBER
NREL/SR-520-33836

11. SUPPLEMENTARY NOTES
NREL Technical Monitor: Harin S. Ullal

12a. DISTRIBUTION/AVAILABILITY STATEMENT
National Technical Information Service
U.S. Department of Commerce
5285 Port Royal Road
Springfield, VA 22161

12b. DISTRIBUTION CODE

13. ABSTRACT *(Maximum 200 words):* Energy Photovoltaics, Inc. (EPV) has consistently pursued a vacuum-based approach to CIGS production, using novel linear-source technology and standard soda-lime glass substrates. It has also chosen to develop processing methods with worker safety in mind. These choices result in layers having controllable purity and low physical defects, and production without significant hazards. Considerations such as these are important in helping to minimize the processing costs of CIGS. Technically, thin-film PV technologies have advanced considerably in the last few years. EPV successfully produced high-quality 0.43m^2 Mo-coated glass substrates that, when cut, enabled NREL to produce 17.1% CIGS cells on such substrates. EPV successfully used novel linear evaporative sources for supply of Cu, In, Ga, and Se to form CIGS on 0.43m^2 substrates, producing modules with V_{oc}'s of up to 37 V. A new approach to buffer-layer deposition was pioneered through synthesis of the compound $ZnIn_2Se_4$ and its use as a source material. In addition, the current generated in exploratory a-Si/a-Si/CIGS stacked devices was increased from 6 to 13 mA/cm^2. Supporting these programs, EPV's upgraded analytical laboratories provided rapid in-house feedback concerning material and device properties. The objective of this subcontract is to develop and assemble the various pieces of new technology that EPV considers essential for cost-effective production of CIGS modules. The long-term objective of the Thin Film PV Partnership Program is to demonstrate low-cost, reproducible modules of 15% aperture-area efficiency.

14. SUBJECT TERMS: PV; CIGS cells; I-V curve; quantum efficiency; manufacturing; junction formation; post-deposition treatment;	15. NUMBER OF PAGES 16. PRICE CODE

17. SECURITY CLASSIFICATION OF REPORT	18. SECURITY CLASSIFICATION OF THIS PAGE	19. SECURITY CLASSIFICATION OF ABSTRACT	20. LIMITATION OF ABSTRACT
Unclassified	Unclassified	Unclassified	UL